AN EXPERIMENTAL INVESTIGATION OF THE INTERNAL BALLISTICS OF SOLID FUEL RAMJETS

Joseph Theodore Phaneuf

NAVAL POSTGRADUATE SCHOOL
Monterey, California

THESIS

An Experimental Investigation of the

Internal Ballistics of Solid Fuel Ramjets

by

Joseph Theodore Phaneuf, Jr.

June 1974

Thesis Advisor: D. W. Netzer

SECURITY CLASSIFICATION OF THIS PAGE (When Data Entered)

REPORT DOCUMENTATION PAGE

READ INSTRUCTIONS BEFORE COMPLETING FORM

1. REPORT NUMBER

2. GOVT ACCESSION NO.

3. RECIPIENT'S CATALOG NUMBER

4. TITLE (and Subtitle)
An Experimental Investigation of the Internal Ballistics of Solid Fuel Ramjets

5. TYPE OF REPORT & PERIOD COVERED
Master's Thesis
June 1974

6. PERFORMING ORG. REPORT NUMBER

7. AUTHOR(s)
Joseph Theodore Phaneuf, Jr.

8. CONTRACT OR GRANT NUMBER(s)

9. PERFORMING ORGANIZATION NAME AND ADDRESS
Naval Postgraduate School
Monterey, California 93940

10. PROGRAM ELEMENT, PROJECT, TASK AREA & WORK UNIT NUMBERS

11. CONTROLLING OFFICE NAME AND ADDRESS
Naval Postgraduate School
Monterey, California 93940

12. REPORT DATE
June 1974

13. NUMBER OF PAGES
87

14. MONITORING AGENCY NAME & ADDRESS(if different from Controlling Office)
Naval Postgraduate School
Monterey, California 93940

15. SECURITY CLASS. (of this report)
Unclassified

15a. DECLASSIFICATION/DOWNGRADING SCHEDULE

16. DISTRIBUTION STATEMENT (of this Report)
Approved for public release; distribution unlimited

17. DISTRIBUTION STATEMENT (of the abstract entered in Block 20, if different from Report)

18. SUPPLEMENTARY NOTES

19. KEY WORDS (Continue on reverse side if necessary and identify by block number)
Ramjet
Solid fuel
Experimental
Internal Ballistics

20. ABSTRACT (Continue on reverse side if necessary and identify by block number)
An experimental investigation of the internal ballistics of solid fuel ramjets was conducted in order to determine the effects of inlet step size, inlet velocity and wall blowing on flow characteristics behind a backward facing step inlet. It was shown that the reattachment point (zone) moves toward the step inlet with wall mass addition at a constant inlet mass flux. For a given step inlet, however, the leading edge of the reattachment zone was stationary with variations in inlet velocity. A point where the wall temperature and centerline static

DD FORM 1 JAN 73 1473 EDITION OF 1 NOV 65 IS OBSOLETE
S/N 0102-014-6601 |
(Page 1)

SECURITY CLASSIFICATION OF THIS PAGE (When Data Entered)

pressure profiles leveled off simultaneously was defined as the end of the reattachment zone. This zone spread out (grew thicker) both with increasing inlet velocity for a given step size, and with increasing step height. Maximum wall temperatures occurred downstream of the reattachment zone.

An Experimental Investigation of the Internal Ballistics of Solid Fuel Ramjets

by

Joseph Theodore Phaneuf, Jr.
Lieutenant Commander, United States Navy
B.S., Naval Postgraduate School, 1973

Submitted in partial fulfillment of the
requirements for the degree of

MASTER OF SCIENCE IN AERONAUTICAL ENGINEERING

from the

NAVAL POSTGRADUATE SCHOOL
June 1974

ABSTRACT

An experimental investigation of the internal ballistics of solid fuel ramjets was conducted in order to determine the effects of inlet step size, inlet velocity and wall blowing on flow characteristics behind a backward facing step inlet.

It was shown that the reattachment point (zone) moves toward the step inlet with wall mass addition at a constant inlet mass flux. For a given step inlet, however, the leading edge of the reattachment zone was stationary with variations in inlet velocity. A point where the wall temperature and centerline static pressure profiles leveled off simultaneously was defined as the end of the reattachment zone. This zone spread out (grew thicker) both with increasing inlet velocity for a given step size, and with increasing step height. Maximum wall temperatures occurred downstream of the reattachment zone.

TABLE OF CONTENTS

LIST OF FIGURES

LIST OF TABLES

I. INTRODUCTION

A research project is currently being conducted at the Naval Postgraduate School to develop a model for the internal ballistics of solid fuel ramjets. Such a model would provide the design engineer with a working tool that would permit performance parameters and operating characteristics to be predicted. The ultimate goals of this project are to develop an analytical model that can be used to predict fuel regression rate and blow-off limits and to experimentally determine the fuel regression rate as a function of operating and configuration variables. Very little experimental data exist that can be used in the determination of the adequacy of such an analytical model.

The means of flame stabilization in solid fuel ramjets was developed originally by the United Technology Center [Ref. 1] . They found that a rearward facing step at the grain inlet provided an adequate flame holder much the same as it does in dump combustors which use liquid fuels. With this step inlet employed, solid fuel ramjet combustors have two distinct combustion zones as shown in Figure 1. In the recirculation zone, products and reactants are mixed, and in the limiting case a well-stirred reactor may be approached. Downstream of the flow reattachment the boundary layer develops and the combustion may be similar to that in a hybrid rocket in which kinetic effects are dominant.

Abbott and Kline [Ref. 2], Krall and Sparrow [Ref. 3], Boaz and Netzer [Ref. 4], and others have investigated the turbulent flow over a

backward facing step. Abbott and Kline found that the recirculation zone behind the backward facing step consisted of a complex pattern of two-dimensional and three-dimensional zones ending at an unsymmetric reattachment point. Their investigation employed water flow through a two-dimensional planar channel. It was found that the location of the reattachment point was not influenced by varying either pipe Reynolds number or inlet turbulence intensity, but did move further downstream when the step height was increased.

Krall and Sparrow also used water flow in their investigation of the flow through an orifice in an electrically heated circular tube. In this constant heat addition axisymmetric experiment, they found that the local heat transfer coefficients in the recirculation, reattachment, and redevelopment zones were several times larger than those for fully developed turbulent pipe flow. The maximum heat transfer coefficient occurred in the vicinity of the reattachment point. Their results were in good agreement with those of Abbott and Kline in that the location of the reattachment point was not affected by changes in Reynolds number. They also found that for small step heights, h, (weak separations or flat recirculation zones) the peak Nusselt number was a well-defined point, but for large step heights (strong separations or thick recirculation zones) the peak Nusselt number spread out into a broad zone. This transition from a well-defined point to a broad zone occurred between $h/D = 0.16$ and $h/D = 0.25$, where D is the pipe diameter. The peak Nusselt number was located between 1.25 and 2.5 pipe diameters downstream of the initial separation. They also found that increasing the step height moved the peak point slightly downstream.

The results of Boaz and Netzer were in general agreement with the results of the above mentioned experimental studies even though air was used as the fluid medium instead of water. Visualization was obtained in a cold air flow through a tube behind a step inlet by injecting a colored fluid mixture at the base of the step. Turbulence in the recirculation zone caused the fluid mixture to be broken up into tiny droplets which collected on the tube walls. Within the region of recirculation, the droplets on the wall moved toward the step face. The droplets were stationary at the flow reattachment point and moved downstream aft of it. Thus, the flow reattachment points were visually measured for several step sizes and Reynolds number conditions. Boaz and Netzer reported that the reattachment point was axially symmetric for most Reynolds number flows. But at high Reynolds numbers, the reattachment point varied around the circumference of the tube, offering a possible explanation of the "spreading out" of the peak Nusselt number reported by Krall and Sparrow.

All of the above investigations considered solid wall geometry with no wall mass addition. Jones, et al [Ref. 5], considered the effects of wall blowing on the recirculation zone flow characteristics using a two-dimensional planar model with schlieren photography. Generally, Jones' data were in good agreement with the other mentioned investigators. He stated that the location of the reattachment point seemed very stable and unaffected by the wall blowing and/or inlet velocities from the qualitative measurements that could be taken from the schlieren photographs.

All of the above investigations were for non-reacting flow conditions. Tests are required for reacting and non-reacting flows in a solid fuel ramjet

geometry in which flow characteristics (i.e., velocity, mass fraction distribution, turbulence intensity, wall temperature profiles, etc.) are measured. Reacting flow measurements are, admittedly, extremely difficult. Therefore, this research was concerned with non-reacting flow in which experiments were conducted in a realistic geometry to simulate a solid fuel ramjet with wall blowing. Air was primarily used as the blowing gas. Helium was used as the blowing gas for the tests in which mass fraction was measured. Helium was used with some reservation, since in a solid fuel ramjet the molecular weight of the wall species can be expected to be somewhat higher than for air.

II. METHOD OF INVESTIGATION

Measurements were taken in non-reacting flows for a variety of conditions using a pressure-jacketed porous bronze tube as the solid fuel ramjet model. Nominal test conditions are listed in Table I. Iron-constantan thermocouples were mounted axially on the porous bronze tube for measurement of temperature profiles along the wall. Velocity measurements were taken utilizing a total pressure rake and a centerline mounted pitot-static probe.

One data set was taken to determine mass fraction profiles by using unheated helium for wall blowing.

All of the data taken were used to determine the location of the reattachment point (zone) and the characteristics of the flow field. The results were compared with the work of previous investigators and with the PISTEP II finite-differencing computer solution for the non-reacting flow field, which is currently under development.

III. DESCRIPTION OF APPARATUS

A. THE BASIC SOLID FUEL RAMJET MODEL

A schematic of the ramjet is shown in Figure 2 and the assembled layout in the photographs of Figures 3, 4, and 5. It consisted of a stainless steel cylindrical jacket in which was axially mounted a porous bronze tube to simulate wall blowing from the solid fuel in the actual motor. A plumbing harness was connected to the external pressure chamber and supplied the input blowing gas as regulated by its own choked orifice device. When air was employed as the blowing gas, it was drawn off from the main air feed system and controlled by a pressure valve to its choked orifice, thereby allowing a constant rate of blowing gas.

The main air feed system was powered by a Pennsylvania air compressor that provided air up to pressures of 150 psia. This air was fed into an air reservoir which could be directly supplied to the ramjet by a manually operated gate valve. When heated inlet air was desired, a Polytherm air heater was used to provide non-vitiated hot air to 500°F.

The ramjet unit itself was axially mounted in the test cell immediately downstream of two pneumatically operated Jamesbury ball valves that either vented main air to the atmosphere or allowed the air to pass through the ramjet. A standard ASME orifice flow meter was used to measure the flow rate of the air to the motor. A manually operated gate valve between the orifice and the motor was used to provide the desired flow rate through the motor.

Line pressure and differential pressure across the ASME orifice were recorded on a Honeywell Model 2106 Visicorder. All twenty-six iron-constantan thermocouples attached to the porous bronze tube, and the iron-constantan thermocouples associated with the ASME orifice and with the choked orifice for blowing-gas flow measurement, were recorded on two Leeds and Northrup multi-print Strip Chart Recorders.

B. FLOW MEASUREMENT WITHIN SIMULATED MOTOR

Two methods of flow measurement were utilized in the experiments: a total pressure rake and a centerline pitot-static probe. The apparatus was also designed to allow the use of miniature hot wire anemometers.

1. Total Pressure Rake

A total pressure rake was designed to axially traverse the porous bronze tube during test runs. Figure 6 is a drawing of the rake installed in the ramjet model. Plastic tubing connected the rake directly to a DATEX SP-101A Pressure Scanner powered by an SRC power supply model 3564. The pressure scanner output was measured by a zero to 15 psig Statham transducer and read on a DIGITEC D. C. millivoltmeter. This setup allowed rapid readings of the seven total and two static pressure probes of the rake. The axially oriented support tube for the rake was scribed for easy determination of probe location when inside the porous bronze tube.

2. Centerline Pitot-Static Probe

A pitot-static probe was designed so that it would fit inter-

changeably with the total pressure rake. Similarly, it was connected to the pressure scanner for rapid readings utilizing the millivoltmeter.

3. Hot Wire Anemometers

Miniature Thermo-Systems Incorporated (TSI) hot wires can be employed for velocity measurement in addition to intensity of turbulence measurements. The configuration of the hot wires in the ramjet model are shown in Figure 7. Figures 5 and 7 also show the hot wire traverse mechanism which was designed to determine the radial position of the hot wire inside the porous bronze tube. The hot wires are connected directly to the TSI calibrating instrument. A CALICO Series 8300 digital multimeter and a true RMS meter are connected so that DC and RMS voltages can be read directly. Additionally, a TEKTRONIX dual beam oscilloscope model R5030 is connected for visual observations of the hot wire output during test runs. Only initial checkout tests were conducted with the hot wires.

C. WALL TEMPERATURE MEASUREMENT

Twenty-six iron-constantan thermocouples were spot welded on the outside wall of the porous bronze tube. They were located on an axial line at points from a distance of one inch from the inlet end at intervals of 0.2 inches. The wires were bundled and fed through a Swagelock fitting access port in the exhaust plate of the ramjet model and connected to two Leeds and Northrup multiprint Strip Chart Recorders. Figure 8 shows the

schematic of the wire-to-tube connections.

D. MASS FRACTION ANALYSIS

Bottled helium was connected to the blowing gas inlet, instead of the compressor air supply, for this test. The pressure rake was used in conjunction with the pressure scanner as before. This time, however, the output of the scanner, instead of being connected to the transducer, was attached by plastic tubing to a gas sampling tank in which was placed a previously calibrated hot wire anemometer. A vacuum pump was employed to evacuate the tank to a constant pressure of four psia. A choked orifice flow plate inserted in the plumbing to the gas sampling tank kept the mass flow rate approximately constant over the entire range of helium and air mass ratios. Changes in hot wire readings gave relative changes in composition of the entrained gas. The hot wire anemometer was connected to the TSI instrument which allowed direct reading of changes in gas composition through the use of the CALICO D. C. multimeter. A schematic of the mass fraction analysis apparatus is shown in Figure 9. Figure 10 is a picture of the assembled hardware.

IV. EXPERIMENTAL PROCEDURE

A. FLOW MEASUREMENTS

Prior to running all tests it was necessary to calibrate the flow measuring devices. The motor air flow rate was measured using an A.S.M.E. sharp-edged orifice. A Visicorder was used to record the line pressure, P_1, and the pressure differential, Δp, across the orifice. A ten-foot water manometer board was employed for calibrating the low ΔP settings, and a mercury manometer for the higher settings. A Heise gauge was used as a secondary standard for calibrating the line pressure, P_1. Air temperatures were measured with a thermocouple and were recorded on a strip chart. The strip chart was specially equipped for recording temperature and was checked for accuracy at both the boiling and freezing points of water.

Line pressure, differential pressure, and line temperature were critical in the accurate measurement of inlet mass flow. Reference 6 outlines in detail the procedures for calculation of mass flow rate across an A.S.M.E. orifice. The equation

$$w_h = 359\ K d^2 F_a Y \sqrt{h_w / \upsilon_1}$$

where

w_h = rate of flow (lbm/hr)

K = flow coefficient, dimensionless; considered a constant for range of Reynolds numbers encountered.

d = diameter of orifice (in)

F_a = thermal expansion factor, dimensionless; considered unity for air.

Y = net expansion factor, dimensionless; varies as h_w/P_1.

h_w = differential pressure (in of H_2O)

v_1 = specific volume at inlet side of orifice (ft^3/lbm).

is that used for calculation of flow rate of a compressible fluid through an orifice.

A sonic choked flow nozzle, described by John [Ref. 7] , was used for controlling and measuring the flow rate of the wall blowing gas. A perfect gas with constant specific heats was assumed to expand isentropically through the nozzle. Operating on the basis that a converging nozzle will remain choked as long as the critical pressure ratio is not exceeded, the required blowing gas line pressure, P_B, was computed for each desired mass flow rate using the equation

$$\dot{m} = \frac{P_t A \sqrt{g_c}\, f(\gamma, M)}{\sqrt{RT_t}}$$

where

$\dot{m}$ = mass flow rate (lbm/sec)

P_t = reservoir pressure = P_B = stagnation pressure (lbf/ft^2)

A = area of convergent nozzle orifice (in^2)

g_c = gravitational constant ($lbm\text{-}ft/lbf\text{-}sec^2$)

R = gas constant ($ft\text{-}lbf/lbm\text{-}°R$)

T_t = stagnation temperature at the nozzle orifice (°R)

and

$$f(\gamma, M)\Big|_{M=1.0} = \gamma \left(\frac{1+\gamma-1}{2}\right)^{\frac{\gamma+1}{2-2\gamma}}$$

where

γ = the ratio of specific heats

B. SUMMARY OF NOMINAL TEST CONDITIONS

Nominal test conditions are summarized in Table I.

TABLE I

NOMINAL TEST CONDITIONS

Air Mass Flow ($\dot{m}$, lbm/sec)	.05	.07	.10	.15
Air Mass Flux (G, lbm/in^2-sec)	.039	.055	.079	.118
Inlet Temperature (°F)	55	200		
Inlet Diameter (in)	.500	.770		
Step (h/D)	.303	.195		
Blowing rate (%$\dot{m}$)	10	10	10	7.5
Blowing choked orifice size (in)	.082(Air)	.143(He)		

C. PROCEDURES FOR COLD INLET AIR TESTS

In runs 1 through 12 flow velocities and temperature profiles were measured for three inlet mass flux conditions. Both wall blowing and non-blowing tests were conducted using the large step size inlet. Alternating rake and centerline pitot probe traverses were made at one-inch intervals from the exhaust plane to the inlet face. Pressure scanner output voltages were displayed on a D. C. millivoltmeter and were recorded at each station along the traverse. The pressure scanner was calibrated

before each set of tests using a mercury manometer. During all runs, main inlet air control parameters were monitored continuously to insure constant mass flux through the motor. Wall blowing mass flow could be initiated or terminated at will by using a hand operated ball valve in close proximity to the motor. During the runs, the strip chart recorders were operated to obtain the wall temperature profiles.

D. PROCEDURES FOR HOT INLET AIR TESTS

In runs 13 through 26 flow velocities and temperature profiles were measured for four inlet mass flux conditions both with and without wall blowing. These tests all used the small step size inlet. The procedure for this set of runs remained the same as for the cold inlet tests.

E. REATTACHMENT ZONE MEASUREMENT

During the testing of runs 1 through 26, it was discovered that the pressure rake outermost probes went through a "plus-zero" to a "minus-zero" zone at about the position where one would expect to find the reattachment point. The downstream edge was taken to be the point where the flow near the wall first moved downstream and the upstream edge where it first moved upstream. Sixteen additional runs were made with the pressure rake and centerline pitot-static probe, with the specific purpose of measuring this "zero-zone" for the four heated inlet mass

flow conditions. These runs were labeled Z1 through Z16. Wall temperature profile data were also collected.

F. MASS FRACTION ANALYSIS

Once the hot wire was calibrated for measuring mass fractions, the procedure for taking the data was relatively simple. The total pressure rake was used in conjunction with the pressure scanner. The gas sampling tank was connected, instead of the usual pressure transducer, to the output side of the scanner. Thus, by keeping the gas sampler plenum chamber at a constant four psia to insure sonic flow through the choked nozzle inlet orifice, it was a simple matter to scan the seven total pressure stations and read the D.C. multimeter for hot wire output voltages. These converted directly into percentages of blowing gas.

Only one actual run was accomplished in the test cell. The amount of bottled helium on hand, and the rate at which ten percent blowing helium depleted the supply, precluded further runs.

Included in Appendix D are the calibration data and the associated curve for the hot wire used in the mass fraction experiment. A special calibration device was designed for this test and is schematically shown in Figure 11. Figure 12 is a picture of the assembled components. Pure helium and air were fed under pressures up to 300 psig into separate holding tanks. From the holding tanks, proportionate parts of each gas

were mixed, according to the percentage of helium desired, by regulating the pressure from each holding tank in consonance with the choked nozzle flow rate formula previously discussed. With a nozzle orifice diameter of 0.020 inches, the helium mass flow was governed by the equation

$$\dot{m}_{He} = 0.0000656 \frac{P}{\sqrt{T}}$$

where P and T are the holding tank pressure and temperature respectively. With a nozzle orifice diameter of 0.0145 inches, the air mass flow was governed by a similar expression

$$\dot{m}_{air} = 0.0000879 \frac{P}{\sqrt{T}}$$

The known mixture mass flow leaving the mixing chamber was routed through the TSI calibration tunnel. A pressure tap on the tunnel wall was used to withdraw the gas sample. The gas passed through the choked nozzle orifice at the inlet of the gas sampling tank, which was evacuated to a constant four psia. The hot wire under calibration was placed in the gas sampler and connected to the CALICO D.C. multimeter via the TSI instrument. Therefore, as gas pressures were regulated according to desired helium percentage, the changes in D.C. voltage reflected the percentage change in helium.

The error estimation for this phase of the research problem is complex enough that it warrants comment at this stage. The mass flow rate formula for isentropic flow through a choked convergent nozzle is a function of total pressure and temperature and the ratio of specific heats. In the calibration procedure, the total pressure and temperature were

static conditions giving a specific mass flow rate through the sampling plenum for each mixture ratio. When the sampling device was connected to the ramjet model, the total pressure was greater than for the calibration because of the velocity head. Thus, for the same mixture ratio, the flow rate in the sampling plenum was higher. This could yield false percentages of helium. An error analysis was done for the case of two percent helium and the results are listed in Table II.

TABLE II

MASS FRACTION ERROR SUMMARY

	calibration	ramjet test
P_t	14.7 psi	14.88 psi (due to velocity)
T_t	532°R	526.5°R
$\dot{m}_{He}$	0.000106 $\frac{lbm}{sec}$	0.000108 $\frac{lbm}{sec}$
V in gas sampler	0.291 $\frac{ft}{sec}$	0.296 $\frac{ft}{sec}$
E^2	4.208	4.210
E	2.051	2.052
%He	15.38	15.43

$\therefore$ .32% change in %He

It is noted that, although the helium percentage changed by less than one percent, the effect would be much more dramatic if the ramjet flow velocity was increased. One possible method to correct this situation would be to cap off the gas sampling tank after drawing off a sample and then take the D.C. multimeter reading. This would eliminate velocity effects and make the hot wire output dependent almost entirely on the thermal conductivity of the mixture.

V. RESULTS AND DISCUSSION

A. REATTACHMENT POINT

Much of the emphasis in this research study was placed on the determination of the location of the reattachment point for flow over a backward facing step at the inlet of a cylindrical tube with and without wall mass addition. Defining a Reynolds number based on the height of the backward facing step as

$$Re_s = \frac{\rho V h}{\mu}$$

where

ρ = fluid density (lbm/ft^3)

V = average velocity at the step inlet (ft/sec)

h = step height (ft)

μ = fluid viscosity (lbm/sec-ft)

it was found that the leading edge of the reattachment zone remained constant for a given step inlet height for most Reynolds numbers. As the step height increased, the leading edge of the reattachment zone moved further downstream. The range of step Reynolds numbers encountered in this study are summarized in Table III.

The results of runs 1 through 26 and Z1 through Z16 are presented in the graphs of Figures 13 through 23. Data from runs 1 through 26 are tabulated in Appendix A. Thermocouple data for all runs in which temperature profiles were plotted are tabulated in Appendix B. The data for runs

TABLE III

SUMMARY OF RANGE OF REYNOLDS NUMBERS (STEP)

h/D \ G [lbm/in^2-sec]	0.039	0.055	0.079	0.118
.303 (COLD)	107,300	141,700	231,800	-----
.195 (COLD)	-----	46,900	58,600	78,200
.195 (HOT)	23,100	35,500	44,100	82,200

Z1 through Z16 are tabulated in Appendix C. The velocity, temperature and centerline static pressure profiles for runs 1 through 26 are plotted on the graphs of Figures 13 through 19. The reattachment zones as well as the wall temperature and centerline static pressure profiles of runs Z1 through Z16 are plotted on the graphs of Figures 20 through 23. These reattachment zones are also superposed on the graphs of runs 13 through 26 for comparative analysis.

The results of the cold inlet flow measurement (runs 1 through 12) that utilized the large step inlet generally were in agreement with the subsequent runs utilizing the small step inlet. The fact that the recirculation zone extended through six inches of the seven-inch porous bronze tube length did not allow any practical analysis of the redevelopment region. The centerline static pressure profiles and velocity profiles did, however, indicate that the reattachment point or zone was located between three and one-half and five inches from the step inlet. The axial location where the centerline static pressure leveled to ambient conditions proved to be a good indicator as to where the end of the reattachment zone was located.

Figure 25 is a drawing of the typical reattachment zone pattern found in these tests. Since these tests were run without an exit nozzle, the velocities attained with this inlet were excessive except at the very low flow rates. Although the recirculation region is relatively extensive, it can be noted from the velocity profiles that the interior pipe flow achieved fully developed turbulent flow at about the same location as the subsequent runs utilizing the larger inlet. It was found that the wall temperature profiles for the cold inlet flow tests had little direct application to the ramjet situation. In these tests, inlet air temperature was less than the blowing air temperature. The noticeable non-symmetry in nearly all of the velocity profiles may partially be explained by the difficulty encountered in maintaining the designed dimensions in the rake itself and the accuracy of keeping it precisely on the centerline of the bronze tube. The pressure rake data have been plotted on the graphs according to the design dimensions between total pressure probes. In addition, the large step inlet may induce non-axisymmetric flow within the tube.

The hot inlet runs, numbered 13 through 26 and Z1 through Z16, were better able to provide information concerning the reattachment point. By reducing the step size, the reattachment zone moved closer to the inlet. This was expected from the results of previous investigators [Refs. 2, 3 and 4] , and provided a better means of interpreting the centerline static pressure profile as well as the more gradual development of the fully developed turbulent pipe flow through the core of the model. Figure 26 is a drawing of the typical reattachment zone pattern of these hot inlet, small step tests. In almost all cases, the centerline static pressure and wall

temperature profiles achieved a definite leveling off point together. This was interpreted to be the end of the reattachment zone, the point at which pure pipe flow begins with its associated boundary layer development. A most significant point is evident from the "zero zone" measurement runs, numbered Z1 through Z8. There is an apparent difference in the beginning of the reattachment zone between tests with blowing and tests without. In all but one case, the "zero zone" moved about 0.3 inches toward the inlet when blowing was introduced with the small step size. This happened at all mass flow rates tested except the highest, which showed a movement of about 0.2 inches toward the inlet with wall blowing. Interestingly, as inlet mass flux increased, the width of the "zero zone" decreased for both blowing and non-blowing tests. However, in both cases, the center of the "zero zone" remained fixed except for high Reynolds number where it moved slightly downstream. It is thought that the "zero zone" leading edge of the reattachment region can physically be described by the illustration in Figure 27. The reattachment zone spreads out downstream with increasing mass flux but the upstream edge remains approximately fixed. It is thought that this spreading out of the reattachment zone possibly results from the increased turbulent transport across the shear line with increased Reynolds number. The fact that increased mixing across the shear line may spread the reattachment zone is observed by comparing Figures 13 and 16. The large h/D and its associated large step Reynolds numbers indicate a much more spread out reattachment zone than the small h/D.

In every case, the maximum wall temperature occurred somewhat further downstream of the apparent end of the reattachment zone as indicated by the simultaneous leveling off of the centerline static pressure and wall temperature profiles. The point of maximum wall temperature varied from about 0.5 inches downstream of the end of the reattachment zone at the lowest inlet mass flux to about 2.0 inches downstream at the highest inlet mass flux. This phenomenon indicates that the point of maximum heat transfer is not coincident with the zone of reattachment and also is dependent upon the inlet mass flux.

Figure 24 compares the data in this investigation with the data of previous investigators. The centers of the "zero zone" regions established by the results of runs Z1 through Z8 were the points plotted for the blowing and non-blowing cases with heated inlet air through the small step inlet. The extent of the spread out reattachment zone is indicated by the short dashed lines. The points chosen for the large step inlet employed are best estimates from careful profile analysis of the graphs of Figures 13 through 15, and from comparison with the reattachment zone characteristics of the small step inlet profiles plotted on Figures 16 through 19. Although the evidence of this investigation indicates a reattachment region is more descriptive of this phenomenon (as indicated in Figure 26), the stagnation point as described in Figure 27 was plotted on the graph of Figure 24 to allow a more analogous comparison with the data of previous investigators.

The unsymmetric reattachment points reported by Abbott and Kline [Ref. 2] are shown. Their work utilizing a two-dimensional channel with water flow showed the flow reattaching at different locations on each side.

They also reported a spreading out of the reattachment point with increased step height as indicated in Figure 24.

Boaz and Netzer used the Krall and Sparrow [Ref. 3] data for the location of maximum heat transfer coefficient to locate the reattachment point. The data of this investigation put it above that of Krall and Sparrow; if peak wall temperature was used to locate the reattachment point, it would be even higher. However, a possible explanation for this significant difference could be the experimental set-up itself. With heated inlet air and a cold tube wall, this study had a variable heat transfer along and toward the wall, as one would expect in solid fuel ramjet combustion. Krall and Sparrow had an electrically heated wall, which fixed the heat transfer rate and directed the heat flow from the wall. Another difference in results reported by Krall and Sparrow was that their peak Nusseit number point moved only slightly downstream with increasing step height, whereas the results of this study, along with the concurrence of the results of Abbott and Kline and of Boaz and Netzer, show that the zone of reattachment moves significantly downstream with increasing step height.

Some additional comments are necessary concerning the experiments conducted in this study. For the non-blowing tests the porous tube had a stagnant plenum surrounding it. This may complicate the temperature profile somewhat when compared with a solid tube wall. In addition, the apparatus used in this experiment provided wall mass addition with practically no pressure drop across the tube wall. Thus, an approximately constant pressure plenum was supplying wall mass addition into a tube in which the static pressure increased in the direction of flow. This

experimental condition would cause non-uniform blowing with more mass addition in the recirculation region than downstream. This is not characteristic of the solid fuel ramjet where mass addition is less in the recirculation region. However, the temperature profiles with and without wall blowing are quite similar, indicating that the non-uniform wall blowing had only small effects. Future tests should perhaps be conducted with the plenum divided into segments in order to provide more realistic ramjet injection rates. An apparatus using this construction is currently being used at the United Technology Center.

The Krall and Sparrow data indicate higher rates of heat transfer in the recirculation region than downstream of the reattachment zone, where the boundary layer develops. However, in the solid fuel ramjet in which chemical reactions occur, the fuel regression rate is a minimum near the inlet and increases to a maximum somewhere downstream or near the reattachment point. Interestingly, the temperature profiles obtained in this study follow closely the fuel regression profiles obtained in the solid fuel ramjet.

Jones, et al [Ref. 5] , using schlieren photography analysis of air flow through a two-dimensional channel, experimented with wall blowing and found no measurable difference in reattachment point location between blowing and non-blowing conditions. The present investigation, however, showed that a small, but significant shift upstream occurred with wall blowing for a constant inlet mass flux.

The results of reattachment point dependence on step inlet size for PISTEP II [Refs. 8 and 9] , the computer solution model, are also plotted

in Figure 24 for the no wall blowing condition. PISTEP II, like Jones' data, predicts little effect of blowing on the flow in the recirculation region and the reattachment point. The results of the initial PISTEP II calculation did, however, show that the reattachment point did move toward the step inlet only slightly with as much as fifty percent wall blowing mass flow rate. Current work with PISTEP II in which more realistic boundary conditions are employed may indicate different results.

The expected uncertainties in the experimental results were calculated using the error analysis method of Kline and McKlintock [Ref. 10]. The calculated uncertainties are summarized in Table IV.

TABLE IV

ERROR ANALYSIS

DEPENDENT VARIABLE	FUNCTION VARIABLES	%ERROR
$\dot{m}$	$\dot{m}(K,d,Fa,Y,h_w,P_1,T_1)$	0.84
$\dot{m}_B$	$\dot{m}_B(P_B,D,T_B)$	1.75
G	$G(\dot{m},D)$	2.63
Re_S	$Re_S(P_S,T_S,\mu,V_S,h)$	5.73
V	$V(\triangle P,T,P)$	2.23

B. MASS FRACTION ANALYSIS

Due to the limited amount of data collected for this phase of the investigation, no definite conclusions were drawn. The mass fraction data are tabulated in Appendix F with the results displayed on the graph of Figure 28. It is interesting to note the unsymmetrical distribution of

helium at the locations sampled. This is indicative of possible strong three-dimensional transport. The apparent centerline of the helium distribution is below that of the geometrical centerline of the tube.

In the lower half of the tube the high percentage of helium is at the wall and decreases radially to a constant value. Axially, the helium percentage increases with distance from the inlet. In the upper half of the tube the radial distribution behaves in the same manner as the lower half. However, the helium content decreases and then increases in the axial direction. As unsymmetrical as it may be, there seems to be a definite pattern to the helium distribution. Both the upper and lower patterns are indicative of wall species accumulating from boundary layer blowing and possibly from helium escaping the recirculation zone. Note that all stations sampled were downstream of the reattachment point where the boundary layer was developing.

VI. CONCLUSIONS AND RECOMMENDATIONS

The primary goal of this investigation was to generate a sufficient amount of accurate reliable data that could be used as a basis for modeling the solid fuel ramjet. The PISTEP II computer program may now be modified through proper choice of boundary conditions to more accurately analyze the recirculation zone and the behavior of the reattachment zone.

During the process of collecting and reducing the data in this investigation, the following conclusions have been drawn:

(1) The leading edge of the reattachment zone, idealized by a pseudo-stagnation point, is upstream of the point where wall temperature and centerline static pressure level off.

(2) The leading edge of the reattachment zone does not move with variations in inlet velocity but the zone itself spreads out with increasing inlet velocity.

(3) Wall blowing moves the leading edge of the reattachment zone upstream.

(4) Maximum wall temperature is located downstream of the reattachment zone and the wall temperature profile closely approximates the fuel regression profile in an actual solid fuel ramjet.

(5) With approximately 10% blowing helium, the mass fraction analysis showed the average helium close to the walls was about 12%, and around the centerline about 6%.

Recommendations to be made are as follows:

(1) Modifications to the gas sampling tank used in the mass fraction analysis are required to avoid errors induced by total velocity head.

(2) Modifications to the plenum chamber which surrounds the porous bronze tube are required so that variable external pressure may be applied to yield an equalized wall mass blowing rate inside the motor model.

APPENDIX A: FLOW MEASUREMENT DATA

RUN #	PROBE	P_1 (PSIA)	T_1 (°F)	ΔP (PSI)	$\dot{m}_{in}$ (LBM/SEC)	P_B (PSIA)	T_B (°F)	$\dot{m}_B$ (LBM/SEC)	STA. (IN)	ΔP (MV)	ΔP (PSI)	P_S (MV)	P_S (PSIA)	ρ (LBM/FT^3)	V (FT/SEC)
1	PITOT	133.0	55	2.38	.1006				0	592	9.47	-91	13.24	.0695	1124
									1	595	9.52	-96	13.16	.0690	1131
									2	553	8.85	-80	13.42	.0704	1080
									3	391	6.26	-54	13.84	.0726	894
									4	171	2.74	-26	14.28	.0749	583
									5	67	1.07	-11	14.52	.0762	361
									6	30	.48	-3	14.65	.0769	241
									7	19	.30	-1	14.68	.0770	190
2	PITOT	133.5	55	2.39	.1009	95	55	.0118	0	616	9.86	-89	13.28	.0697	1145
									1	606	9.70	-91	13.24	.0695	1138
									2	560	8.96	-75	13.50	.0708	1083
									3	400	6.40	-50	13.90	.0729	902
									4	185	2.96	-25	14.30	.0750	605
									5	75	1.20	-10	14.54	.0763	382
									6	35	.56	-2	14.67	.0770	260
									7	23	.37	-1	14.68	.0770	211
7	PITOT	132.8	55	1.21	.0719				0	248	3.97	-45	13.98	.0733	709
									1	248	3.97	-47	13.95	.0732	709
									2	214	3.42	-35	14.14	.0742	654
									3	127	2.03	-20	14.38	.0754	500
									4	50	.80	-8	14.57	.0764	312
									5	19	.30	-2	14.67	.0769	190
									6	9	.14	0	14.70	.0771	130
									7	7	.11	0	14.70	.0771	115

APPENDIX A: FLOW MEASUREMENT DATA

RUN #	PROBE	P_1 (PSIA)	T_1 (°F)	ΔP (PSI)	$\dot{m}_{in}$ $\frac{(LBM)}{SEC}$	P_B (PSIA)	T_B (°F)	$\dot{m}_B$ $\frac{(LBM)}{SEC}$	STA. (IN)	ΔP (MV)	ΔP (PSI)	P_S (MV)	P_S (PSIA)	ρ $\frac{(LBM)}{FT^3}$	V $\frac{(FT)}{SEC}$
8	PITOT	129.0	55	1.18	.0700	71	58	.00877	0	236	3.78	-41	14.04	.0737	690
									1	237	3.79	-42	14.03	.0736	691
									2	215	3.44	-34	14.16	.0743	655
									3	148	2.37	-21	14.36	.0754	540
									4	65	1.04	-9	14.56	.0764	355
									5	26	.42	-3	14.65	.0769	225
									6	13	.21	0	14.70	.0771	159
									7	8	.13	0	14.70	.0771	125
9	PITOT	139.5	55	.57	.0506				0	129	2.06	-24	14.32	.0751	504
									1	128	2.05	-25	14.30	.0750	503
									2	104	1.66	-17	14.43	.0757	451
									3	55	.88	-8	14.57	.0764	327
									4	20	.32	-2	14.67	.0769	196
									5	8	.13	0	14.70	.0771	125
									6	5	.08	0	14.70	.0771	98
									7	4	.06	0	14.70	.0771	85
10	PITOT	139.0	55	.57	.0505	55	55	.0068	0	142	2.27	-24	14.32	.0751	529
									1	141	2.26	-25	14.30	.0750	528
									2	115	1.84	-17	14.43	.0757	475
									3	63	1.01	-8	14.57	.0764	350
									4	24	.38	-2	14.67	.0769	214
									5	10	.16	0	14.70	.0771	139
									6	7	.11	0	14.70	.0771	115
									7	5	.08	0	14.70	.0771	98

APPENDIX A: FLOW MEASUREMENT DATA

RUN #	PROBE	P_1 (PSIA)	T_1 (°F)	ΔP (PSI)	$\dot{m}_{in}$ (LBM/SEC)	P_B (PSIA)	T_B (°F)	$\dot{m}_B$ (LBM/SEC)	STA. (IN)	ΔP (MV)	ΔP (PSI)	P_S (MV)	P_S (PSIA)	Q (LBM/FT^3)	V (FT/SEC)
15	PITOT	131	168	2.9	.0997				0	106	1.70	-25	14.30	.0615	506
									1	100	1.60	-15	14.46	.0622	488
									2	95	1.52	-10	14.54	.0626	475
									3	77	1.23	-4	14.64	.0630	426
									4	50	.80	0	14.70	.0632	343
									5	33	.53	0	14.70	.0632	279
									6	25	.40	0	14.70	.0632	242
									7	21	.34	0	14.70	.0632	223
16	PITOT	131	170	2.9	.0995	95	55	.0118	0	111	1.78	-18	14.41	.0618	517
									1	96	1.54	-5	14.62	.0627	477
									2	79	1.26	0	14.70	.0630	431
									3	79	1.26	0	14.70	.0630	431
									4	55	.88	2	14.73	.0632	359
									5	38	.61	1	14.72	.0632	299
									6	29	.46	1	14.72	.0632	260
									7	25	.40	0	14.70	.0630	243
17	PITOT	134.5	223	1.54	.0708				0	67	1.07	-22	14.35	.0568	418
									1	54	.86	-11	14.52	.0574	373
									2	44	.70	-4	14.64	.0579	335
									3	36	.58	-1	14.68	.0581	304
									4	24	.38	0	14.70	.0582	246
									5	16	.26	0	14.70	.0582	204
									6	12	.19	0	14.70	.0582	174
									7	11	.18	0	14.70	.0582	169

APPENDIX A: FLOW MEASUREMENT DATA

RUN #	PROBE	P_1 (PSIA)	T_1 (°F)	ΔP (PSI)	$\dot{m}_{in}$ $\frac{(LBM)}{SEC}$	P_B (PSIA)	T_B (°F)	$\dot{m}_B$ $\frac{(LBM)}{SEC}$	STA. (IN)	ΔP (MV)	ΔP (PSI)	P_S (MV)	P_S (PSIA)	ρ $\frac{(LBM)}{FT^3}$	V $\frac{(FT)}{SEC}$
18	PITOT	134	225	1.54	.0706	71	62	.0087	0	63	1.01	-17	14.43	.0569	406
									1	54	.86	-8	14.57	.0575	372
									2	47	.75	-2	14.67	.0579	347
									3	39	.62	0	14.70	.0580	315
									4	28	.45	1	14.72	.0580	268
									5	20	.32	0	14.70	.0580	226
									6	15	.24	0	14.70	.0580	196
									7	13	.21	0	14.70	.0580	183
23	PITOT	131.5	200	.75	.0499				0	28	.45	-9	14.56	.0596	265
									1	24	.38	-5	14.62	.0598	242
									2	21	.34	-2	14.67	.0601	229
									3	17	.27	0	14.70	.0602	204
									4	12	.19	0	14.70	.0602	171
									5	8	.13	0	14.70	.0602	142
									6	6	.10	0	14.70	.0602	124
									7	5	.08	0	14.70	.0602	111
24	PITOT	132	199.5	.74	.0495	55	61.5	.0068	0	30	.48	-8	14.57	.0597	273
									1	26	.42	-4	14.64	.0600	255
									2	23	.37	-1	14.68	.0602	239
									3	20	.32	0	14.70	.0602	222
									4	15	.24	0	14.70	.0602	192
									5	10	.16	0	14.70	.0602	157
									6	8	.13	0	14.70	.0602	142
									7	7	.11	0	14.70	.0602	130

APPENDIX A: FLOW MEASUREMENT DATA

RUN #	PROBE	P_1 (PSIA)	T_1 (°F)	ΔP (PSI)	$\dot{m}_{in}$ $\frac{(LBM)}{SEC}$	P_B (PSIA)	T_B (°F)	$\dot{m}_B$ $\frac{(LBM)}{SEC}$	STA. (IN)	ΔP (MV)	ΔP (PSI)	P_S (MV)	P_S (PSIA)	ρ $\frac{(LBM)}{FT^3}$	V $\frac{(FT)}{SEC}$
25	PITOT	125	230	7.49	.148				0	322	5.15	-98	13.13	.0514	964
									1	289	4.62	-67	13.63	.0534	896
									2	252	4.03	-33	14.17	.0555	821
									3	213	3.41	-17	14.43	.0565	748
									4	143	2.29	-6	14.60	.0572	609
									5	90	1.44	-3	14.65	.0574	482
									6	62	.99	0	14.70	.0576	399
									7	49	.78	-1	14.68	.0575	355
26	PITOT	126	233.5	7.49	.148	95	61	.0117	0	319	5.10	-86	13.32	.0519	955
									1	286	4.58	-55	13.82	.0538	889
									2	255	4.08	-24	14.32	.0558	824
									3	219	3.50	-11	14.52	.0566	757
									4	151	2.42	-2	14.67	.0571	627
									5	98	1.57	0	14.70	.0573	504
									6	70	1.12	1	14.72	.0573	426
									7	60	.96	-1	14.68	.0572	395

	STA	6 inches			5 inches			4 inches		
		$\triangle P$ (MV)	$\triangle P$ (PSI)	V (FPS)	$\triangle P$ (MV)	$\triangle P$ (PSI)	V (FPS)	$\triangle P$ (MV)	$\triangle P$ (PSI)	V (FPS)
Run # 3 Rake	1	14	.22	162	9	.14	129	-		
P_1 132.8 PSIA	2	15	.24	169	17	.27	180	16	.26	177
T_1 55 °F	3	29	.46	234	49	.78	305	96	1.54	432
$\triangle P$ 2.35 PSI	4	35	.56	258	69	1.10	362	175	2.82	584
$\dot{m}_{in}$ .0999 LBM/SEC	5	31	.50	244	52	.83	315	119	1.90	479
P_B PSIA	6	19	.30	189	21	.34	205	29	.46	236
T_B °F	7	14	.22	162	9	.14	129	-		
$\dot{m}_B$ LBM/SEC	P_S		ρ : LBM/FT^3			ρ : LBM/FT^3			ρ : LBM/FT^3	
	11	5	.0778		-1	.0770		-16	.0758	
	12	5			-1			-16		
Run # 4 Rake	1	13	.21	160	8	.13	125	-		
P_1 129.5 PSIA	2	18	.29	187	19	.30	191	-		
T_1 55 °F	3	40	.64	278	74	1.18	378	132	2.11	505
$\triangle P$ 2.37 PSI	4	54	.86	323	115	1.84	472	261	4.18	711
$\dot{m}_{in}$ .1002 LBM/SEC	5	45	.72	295	81	1.30	397	164	2.62	563
P_B 95 PSIA	6	24	.38	215	26	.42	226	32	.51	249
T_B 58 °F	7	15	.24	170	9	.14	130	-		
$\dot{m}_B$ .0117 LBM/SEC	P_S		ρ : LBM/FT^3			ρ : LBM/FT^3			ρ : LBM/FT^3	
	11	6	.0766		-4	.0768		-23	.0752	
	12	6			-4			-23		

	STA	6 inches			5 inches			4 inches		
		ΔP (MV)	ΔP (PSI)	V (FPS)	ΔP (MV)	ΔP (PSI)	V (FPS)	ΔP (MV)	ΔP (PSI)	V (FPS)
Run #5 Rake	1	9	.14	129	7	.11	115	4	.06	85
P_1 134.5 PSIA	2	9	.14	129	8	.13	125	8	.13	125
T_1 55 °F	3	10	.16	138	17	.27	180	35	.56	260
△P 1.18 PSI	4	13	.21	159	23	.37	211	57	.91	332
$\dot{m}_{in}$ .0715 LMB/SEC	5	11	.18	147	18	.29	187	43	.69	289
P_B PSIA	6	8	.13	125	10	.16	139	13	.21	159
T_B °F	7	7	.11	115	9	.14	130	4	.06	85
$\dot{m}_B$ LBM/SEC	P_S									
	11	4	ρ : LBM/FT^3		1	ρ : LBM/FT^3		-4	ρ : LBM/FT^3	
	12	4	.0775		1	.0772		-4	.0768	
Run #6 Rake	1	8	.13	125	7	.11	115	-		
P_1 135 PSIA	2	8	.13	125	9	.14	130	8	.13	125
T_1 55 °F	3	12	.19	151	20	.32	196	43	.69	289
△P 1.18 PSI	4	15	.24	170	27	.43	227	74	1.18	377
$\dot{m}_{in}$ .0716 LBM/SEC	5	14	.22	162	22	.35	205	52	.83	317
P_B 71 PSIA	6	11	.18	147	12	.19	151	14	.22	163
T_B 60 °F	7	9	.14	129	8	.13	125	4	.06	85
$\dot{m}_B$ .00875 LBM/SEC	P_S		ρ : LBM/FT^3			ρ : LBM/FT^3			ρ : LBM/FT^3	
	11	5	.0775		2	.0773		-4	.0768	
	12	5			2			-4		

	STA	6 inches			5 inches			4 inches		
		△P (MV)	△P (PSI)	V (FPS)	△P (MV)	△P (PSI)	V (FPS)	△P (MV)	△P (PSI)	V (FPS)
Run # 11 Rake	1	4.5	.07	92	3.5	.06	85	1	.02	49
P_1 136 PSIA	2	4.5	.07	92	5.5	.09	104	5	.08	98
T_1 55 °F	3	5.5	.09	104	8.5	.14	130	15	.24	170
△P 0.585 PSI	4	6.5	.10	110	16.5	.26	177	24	.38	214
$\dot{m}_{in}$ .0506 LBM/SEC	5	5.5	.09	104	9.5	.15	134	17	.27	180
P_B PSIA	6	4.5	.07	92	5.5	.09	104	3	.05	78
T_B °F	7	4.5	.07	92	4.5	.07	92	1	.02	49
$\dot{m}_B$ LBM/SEC	P_S		ρ : LBM/FT^3			ρ : LBM/FT^3			ρ : LBM/FT^3	
	11	1	.0772		0	.0772		0	.0771	
	12	2			1			0		
Run # 12 Rake	1	5	.08	98	4.5	.07	92	2	.03	60
P_1 135.5 PSIA	2	5	.08	98	6.5	.10	110	5	.08	98
T_1 55 °F	3	6	.10	110	10.5	.17	143	15	.24	170
△P .585 PSI	4	7	.11	115	12.5	.20	155	24	.38	214
$\dot{m}_{in}$ .0505 LBM/SEC	5	7	.11	115	10.5	.17	143	18	.29	187
P_B 55 PSIA	6	5	.08	98	6.5	.10	110	4	.06	85
T_B 57 °F	7	5	.08	98	5.5	.09	104	2	.03	60
$\dot{m}_B$ .0068 LBM/SEC	P_S									
	11	2	ρ: LBM/FT^3		0	ρ : LBM/FT^3		0	ρ : LBM/FT^3	
	12	2	.0773		1	.0772		0	.0771	

	STA	3 inches			2 inches			1 inches		
		ΔP (MV)	ΔP (PSI)	V (FPS)	ΔP (MV)	ΔP (PSI)	V (FPS)	ΔP (MV)	ΔP (PSI)	V (FPS)
Run # 11 Rake		-								
P_1 136 PSIA		4.5	.07	92						
T_1 55 °F		31.5	.50	246						
Δ P 0.585 PSI		57.5	.92	334						
$\dot{m}_{in}$ .0506 LBM/SEC		32.5	.52	251						
P_B PSIA		-								
T_B °F		-								
$\dot{m}_B$ LBM/SEC			ρ : LBM/FT^3			ρ : LBM/FT^3			ρ : LBM/FT^3	
		-4	.0767							
		-5								
Run # 12 Rake		-								
P_1 135.5 PSIA		4	.06	85						
T_1 55 °F		31	.50	246						
Δ P .585 PSI		57	.91	331						
$\dot{m}_{in}$ .0505 LBM/SEC		33	.53	253						
P_B 55 PSIA		4	.06	85						
T_B 57 °F		-								
$\dot{m}_B$ .0068 LBM/SEC		-3	ρ : LBM/FT^3			ρ : LBM/FT^3			ρ : LBM/FT^3	
		-5	.0768							

	STA	6 inches			5 inches			4 inches		
		$\triangle P$ (MV)	$\triangle P$ (PSI)	V (FPS)	$\triangle P$ (MV)	$\triangle P$ (PSI)	V (FPS)	$\triangle P$ (MV)	$\triangle P$ (PSI)	V (FPS)
Run # 13 Rake	1	16.5	.26	191	15.5	.25	188	13	.21	172
P_1 132 PSIA	2	18.5	.30	206	20.5	.33	216	22	.35	223
T_1 151 °F	3	25.5	.41	240	32.5	.52	271	43	.69	312
$\triangle P$ 2.90 PSI	4	29.5	.47	257	38.5	.62	296	57	.91	359
$\dot{m}_{in}$ .1015 LBM/SEC	5	26.5	.42	243	33.5	.54	276	47	.75	326
P_B PSIA	6	20.5	.33	216	21.5	.34	219	21	.34	219
T_B °F	7	18.5	.30	206	17.5	.28	199	15	.24	184
$\dot{m}_B$ LBM/SEC	P_S		ρ : LBM/FT^3			ρ : LBM/FT^3			ρ : LBM/FT^3	
	11	9	.0657		7	.0656		6	.0655	
	12	12			10			8		
Run # 14 Rake	1	18.5	.30	207	17.5	.28	199	14.5	.23	181
P_1 131 PSIA	2	21.5	.34	220	22.5	.36	226	23.5	.38	232
T_1 156 °F	3	30.5	.50	267	36.5	.58	287	48.5	.78	333
$\triangle P$ 2.90 PSI	4	33.5	.54	277	43.5	.70	315	62.5	1.00	377
$\dot{m}_{in}$ .1006 LBM/SEC	5	31.5	.50	267	37.5	.60	292	50.5	.81	339
P_B 95 PSIA	6	24.5	.39	236	24.5	.39	235	24.5	.39	235
T_B 55 °F	7	20.5	.33	217	19.5	.31	210	17.5	.28	199
$\dot{m}_B$ .0118 LBM/SEC	P_S		ρ : LBM/FT^3			ρ : LBM/FT^3			ρ : LBM/FT^3	
	11	13	.0652		11	.0653		10	.0653	
	12	16			14			13		

STA	3 inches			2 inches			1 inches		
	ΔP (MV)	ΔP (PSI)	V (FPS)	ΔP (MV)	ΔP (PSI)	V (FPS)	ΔP (MV)	ΔP (PSI)	V (FPS)
Run # 13 Rake	8	.13	136	0	0	0	-		
P_1 132 PSIA	22	.35	223	21	.34	220	21.5	.34	222
T_1 151 °F	64	1.02	380	90	1.44	453	115.5	1.85	518
Δ P 2.90 PSI	85	1.36	439	102	1.63	482	117.5	1.88	522
$\dot{m}_{in}$ .1015 LBM/SEC	65	1.04	384	87	1.39	445	116.5	1.86	519
P_B PSIA	22	.35	223	23	.37	230	20.5	.33	219
T_B °F	9	.14	141	0	0	0	-		
$\dot{m}_B$ LBM/SEC		ρ :LBM/FT^3			ρ :LBM/FT^3			ρ : LBM/FT^3	
	3	.0653		0	.0650		-12	.0640	
	5			0			-15		
Run # 14 Rake	11.5	.18	160	4	.06	93	-		
P_1 131 PSIA	23.5	.38	233	20	.32	214	20.5	.33	219
T_1 156 °F	67.5	1.08	392	94	1.50	463	118.5	1.90	525
Δ P 2.90 PSI	89.5	1.43	451	106	1.70	493	119.5	1.91	526
$\dot{m}_{in}$ .1006 LBM/SEC	67.5	1.08	392	90	1.44	454	118.5	1.90	525
P_B 95 PSIA	25.5	.41	242	27	.43	248	26.5	.42	247
T_B 55 °F	12.5	.20	169	1	.02	54			
$\dot{m}_B$ .0118 LBM/SEC		ρ : LBM/FT^3			ρ : LBM/FT^3			ρ : LBM/FT^3	
	7	.0651		3	.0648		-6	.0640	
	10			5			-9		

	STA	6 inches			5 inches			4 inches		
		△P (MV)	△P (PSI)	V (FPS)	△P (MV)	△P (PSI)	V (FPS)	△P (MV)	△P (PSI)	V (FPS)
Run # 19 Rake	1	8.5	.14	149	8	.13	144	7	.11	132
P_1 133 PSIA	2	9.5	.15	154	10	.16	160	11	.18	169
T_1 225 °F	3	12.5	.20	178	15	.24	195	22	.35	236
△ P 1.53 PSI	4	13.5	.22	187	18	.29	215	28	.45	268
$\dot{m}_{in}$ .0700 LBM/SEC	5	12.5	.20	178	16	.26	203	23	.37	243
P_B PSIA	6	10.5	.17	164	11	.18	169	12	.19	174
T_B °F	7	8.5	.14	149	8	.13	144	7	.11	132
$\dot{m}_B$ LBM/SEC	P_S									
	11	7	ρ : LBM/FT^3		5	ρ : LBM/FT^3		4	ρ : LBM/FT^3	
	12	6	.0584		5	.0583		4	.0582	
Run # 20 Rake	1	9	.14	149	8	.13	144	6.5	.10	126
P_1 132 PSIA	2	11	.18	169	11	.18	169	13.5	.22	187
T_1 225 °F	3	14	.22	187	17	.27	207	23.5	.38	246
△ P 1.53 PSI	4	16	.26	203	21	.34	232	31.5	.50	282
$\dot{m}_{in}$ .0698 LBM/SEC	5	15	.24	195	18	.29	215	26.5	.42	258
P_B 71 PSIA	6	11	.18	169	12	.19	174	11.5	.18	169
T_B 63 °F	7	10	.16	159	9	.14	149	8.5	.14	149
$\dot{m}_B$ .0087 LBM/SEC	P_S		ρ : LBM/FT^3			ρ : LBM/FT^3			ρ :LBM/FT^3	
	11	8	.0585		7	.0584		7	.0584	
	12	8			7			6		

	STA	3 inches			2 inches			1 inches		
		ΔP (MV)	ΔP (PSI)	V (FPS)	ΔP (MV)	ΔP (PSI)	V (FPS)	ΔP (MV)	ΔP (PSI)	V (FPS)
Run # 19 Rake		5	.08	113	0	0	0	-		
P_1 133 PSIA		13	.21	183	13	.21	183	26.5	.42	261
T_1 225 °F		31	.50	283	44	.70	335	59.5	.95	392
Δ P 1.53 PSI		42	.67	327	50	.80	358	61.5	.98	398
$\dot{m}_{in}$ .0700 LBM/SEC		32	.51	285	43	.69	332	60.5	.97	396
P_B PSIA		12	.19	174	12	.19	174	17.5	.28	213
T_B °F		5	.08	113	0	0	0	-		
$\dot{m}_B$ LBM/SEC										
		2	ρ : LBM/FT^3		0	ρ : LBM/FT^3		-10	ρ : LBM/FT^3	
		2	.0581		0	.0580		-9	.0574	
Run # 20 Rake		5	.08	113	1	.02	57	-		
P_1 132 PSIA		14	.22	187	15	.24	196	25.5	.41	257
T_1 225 °F		35	.56	298	47	.75	346	60.5	.97	395
Δ P 1.53 PSI		47	.75	345	54	.86	371	62.5	1.00	401
$\dot{m}_{in}$ .0698 LBM/SEC		37	.59	306	47	.75	346	61.5	.98	397
P_B 71 PSIA		13	.21	183	14	.22	187	14.5	.23	192
T_B 63 °F		6	.10	126	0	0	0	-		
$\dot{m}_B$ .0087 LBM/SEC			ρ : LBM/FT^3			ρ : LBM/FT^3			ρ : LBM/FT^3	
		5	.0583		2	.0581		-6	.0576	
		5			2			-5		

	STA	6 inches			5 inches			4 inches		
		$\triangle P$ (MV)	$\triangle P$ (PSI)	V (FPS)	$\triangle P$ (MV)	$\triangle P$ (PSI)	V (FPS)	$\triangle P$ (MV)	$\triangle P$ (PSI)	V (FPS)
Run # 21 Rake	1	4	.06	97	3	.05	89	3	.05	89
P_1 133 PSIA	2	5	.08	112	5	.08	112	6	.10	125
T_1 216 °F	3	6	.10	125	7	.11	132	11	.18	168
$\triangle P$ .77 PSI	4	7	.11	132	9	.14	149	16	.26	202
$\dot{m}_{in}$ .0503 LBM/SEC	5	7	.11	132	8	.13	143	13	.21	182
P_B PSIA	6	5	.08	112	5	.08	112	5	.08	112
T_B °F	7	5	.08	112	4	.06	97	4	.06	97
$\dot{m}_B$ LBM/SEC	P_S		ρ : LBM/FT^3			ρ : LBM/FT^3			ρ : LBM/FT^3	
	11	3	.0589		3	.0589		2	.0589	
	12	3			3			2		
Run # 22 Rake	1	4.5	.07	104	5.5	.09	118	4.5	.07	105
P_1 133 PSIA	2	5.5	.09	118	6.5	.10	125	7.5	.12	137
T_1 210 °F	3	8.5	.14	148	10.5	.17	163	14.5	.23	189
$\triangle P$ .77 PSI	4	8.5	.14	148	12.5	.20	177	19.5	.31	220
$\dot{m}_{in}$ .0505 LBM/SEC	5	8.5	.14	148	11.5	.18	168	14.5	.23	189
P_B 55 PSIA	6	6.5	.10	125	7.5	.12	137	7.5	.12	137
T_B 83 °F	7	5.5	.09	118	5.5	.09	118	4.5	.07	105
$\dot{m}_B$ .0066 LBM/SEC	P_S									
	11	4	ρ : LBM/FT^3		3	ρ :LBM/FT^3		3	ρ : LBM/FT^3	
	12	5	.0596		4	.0595		4	.0595	

	STA	3 inches			2 inches			1 inches		
		$\triangle P$ (MV)	$\triangle P$ (PSI)	V (FPS)	$\triangle P$ (MV)	$\triangle P$ (PSI)	V (FPS)	$\triangle P$ (MV)	$\triangle P$ (PSI)	V (FPS)
Run # 21 Rake		1	.02	35	-			-		
P_1 133 PSIA		7	.11	132	8	.13	143	13.5	.22	186
T_1 216 °F		16	.26	203	22	.35	235	28.5	.46	269
$\triangle P$ .77 PSI		22	.35	235	25	.40	251	28.5	.46	269
$\dot{m}_{in}$ .0503 LBM/SEC		17	.27	206	23	.37	242	28.5	.46	269
P_B PSIA		5	.08	112	4	.06	97	5.5	.09	119
T_B °F		2	.03	69	-			-		
$\dot{m}_B$ LBM/SEC			ρ : LBM/FT^3			ρ : LBM/FT^3			ρ : LBM/FT^3	
		1	.0588		0	.0588		-4	.0585	
		1			0			-3		
Run # 22 Rake		3.5	.06	97	0	0	0	-		
P_1 133 PSIA		7.5	.12	137	9	.14	148	20	.32	224
T_1 210 °F		19.5	.31	220	25	.40	250	29	.46	267
$\triangle P$ .77 PSI		24.5	.39	247	28	.45	265	30	.48	274
$\dot{m}_{in}$ .0505 LBM/SEC		19.5	.31	220	26	.42	256	29	.46	267
P_B 55 PSIA		7.5	.12	137	7	.11	131	0	0	0
T_B 83 °F		3.5	.06	97	0	0	0	-		
$\dot{m}_B$ .0066 LBM/SEC										
		2	ρ : LBM/FT^3		0	ρ : LBM/FT^3		-2	ρ : LBM/FT^3	
		3	.0594		0	.0593		-2	.0591	

Appendix A

Voltage vs. Pressure

Calibration Curve

(PSI = 1.6 x MV)

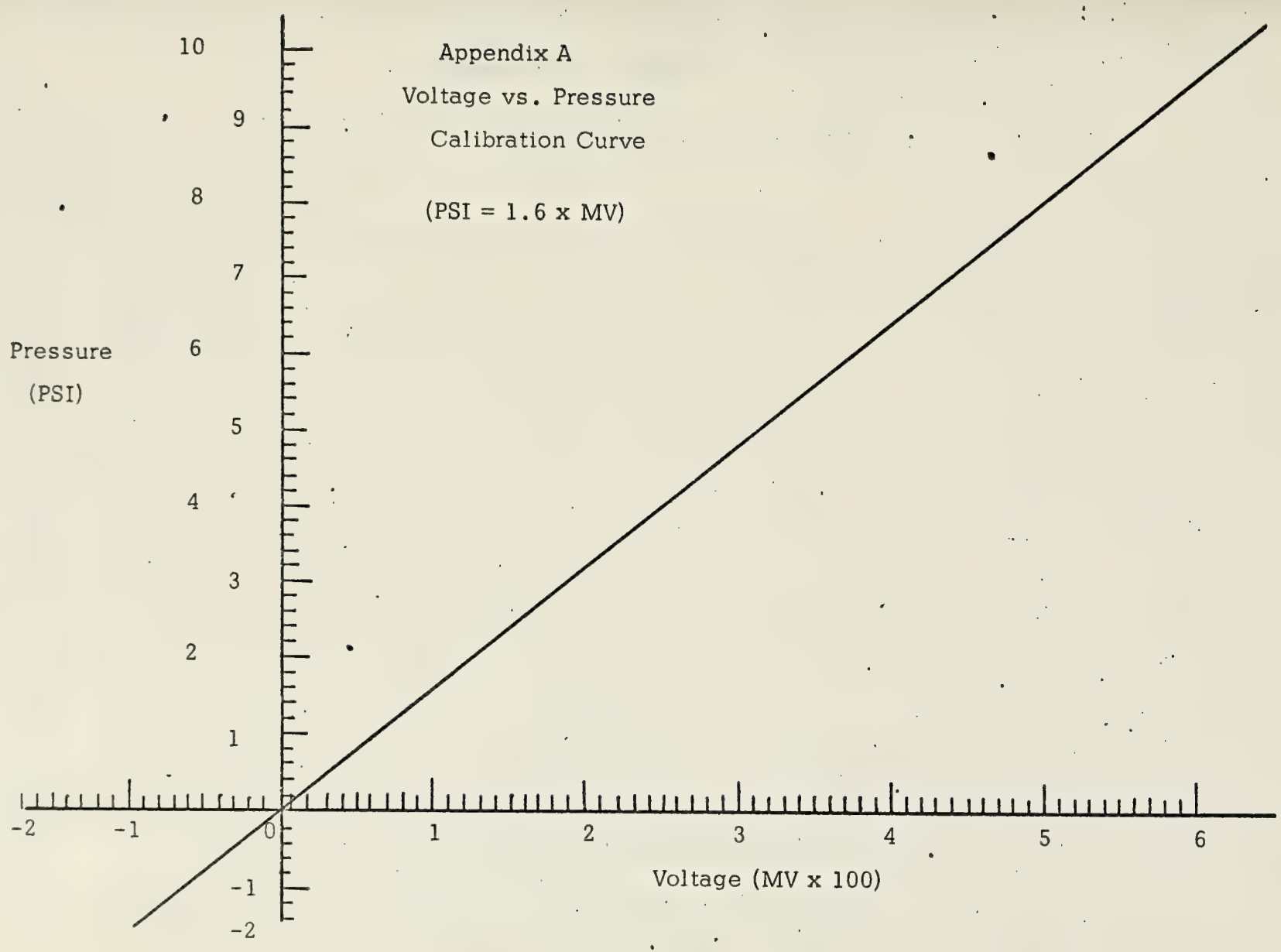

APPENDIX B: TEMPERATURE PROFILE DATA

RUNS IN WHICH TEMPERATURE DATA WERE TAKEN AND PLOTTED (°F)

Thermo Couple #	3	4	5	6	11	12	13	14	19	20	21	22	25	26	Z9	Z10	Z11	Z12	Z13	Z14	Z15	Z16
1	54	58	54	57	55	54	119	94	176	121	171	124	193	130	164	136	181	126	186	120	184	119
2	54	58	54	57	55	54	121	97	181	126	174	128	196	134	167	138	183	132	188	126	185	123
3	53	58	54	57	55	54	123	101	184	131	176	132	198	139	171	141	185	136	189	132	185	129
4	53	58	54	57	55	54	127	105	186	136	181	137	199	144	173	144	185	141	189	138	185	135
5	53	58	54	57	55	54	129	108	189	139	183	139	201	148	175	145	186	144	190	142	185	141
6	52	58	54	57	55	54	132	112	191	144	184	142	201	156	177	148	188	148	192	148	186	149
7	52	58	54	57	55	54	133	115	192	148	186	143	202	161	178	149	188	151	192	152	186	154
8	51	57	54	57	55	54	134	118	193	152	187	144	204	168	179	151	189	152	192	160	187	161
9	51	56	54	56	55	54	134	119	195	154	187	145	204	174	180	151	189	154	192	164	188	167
10	51	55	54	56	55	54	134	120	195	157	189	145	204	179	180	152	189	156	193	169	188	171
11	50	55	54	55	55	54	134	120	196	160	189	147	205	184	180	152	189	158	193	171	190	175
12	50	54	54	55	55	54	134	118	196	160	189	147	206	189	180	152	189	158	193	172	190	178
13	50	53	54	55	55	54	134	118	197	160	189	147	206	192	180	152	189	159	193	172	190	180
14	50	53	54	55	55	54	135	119	197	160	189	146	206	194	181	153	189	161	194	175	190	181
15	50	53	54	54	55	54	135	121	197	162	190	145	206	196	181	154	189	162	194	175	190	182
16	50	52	54	54	55	54	135	121	198	160	190	144	207	199	181	153	189	162	194	175	190	183
17	50	52	54	54	55	54	136	121	198	157	190	142	207	200	181	152	189	162	194	175	190	185
18	50	52	54	54	55	54	136	122	199	157	190	142	207	201	181	152	189	162	194	175	190	185
19	51	53	54	54	55	54	137	121	199	157	190	141	209	201	181	152	189	162	194	175	190	185
20	51	53	54	54	55	54	137	121	199	156	190	138	209	201	181	151	189	162	194	175	190	185
21	52	53	54	54	55	54	137	121	199	156	190	137	209	204	181	151	189	162	194	175	190	186
22	52	54	54	55	55	54	137	121	199	157	190	137	209	204	181	151	189	162	194	175	190	186
23	52	54	54	55	55	54	138	121	199	157	189	137	209	204	180	151	189	161	194	174	190	186
24	53	54	55	55	55	54	138	120	199	157	189	137	209	204	180	150	189	161	194	174	190	186
25	53	54	55	55	55	54	138	119	197	156	189	137	203	203	180	151	189	161	194	174	190	186
26	53	54	55	55	55	54	138	119	195	156	187	137	209	203	180	151	189	161	194	174	190	186

APPENDIX C: REATTACHMENT "ZERO ZONE" DATA

RUN #	PROBE	P_1 (PSIA)	T_1 (°F)	$\triangle P$ (PSI)	$\dot{m}$ (LBM/SEC)	P_B (PSIA)	T_B (°F)	$\dot{m}_B$ (LBM/SEC)	AXIAL DISTANCE (INCHES) -0MV	+0MV
Z1	PITOT	131	195	.74	.0495				2.10	2.56
Z2	PITOT	132	195	.74	.0497	40	55	.00495	1.80	2.22
Z3	PITOT	131	190	1.45	.0695				2.17	2.39
Z4	PITOT	131	185	1.45	.0698	56	55	.00693	1.01	2.09
Z5	PITOT	132	189	3.00	.100				2.32	2.38
Z6	PITOT	132	194	3.00	.100	80	55	.00991	1.95	2.03
Z7	PITOT	132	193	6.8	.1490				2.38	2.44
Z8	PITOT	132	195	6.8	.1487	95	55	.0118	2.15	2.18

									STA (IN)	P_S (MV)	P_S (PSIA)
Z9	PITOT	131	210	.75	.0493				0	-8	14.57
									1	-4	14.64
									2	-1	14.68
									3	0	14.70
									4	0	14.70
									5	0	14.70
									6	0	14.70
									7	0	14.70
Z10	PITOT	131	206	.75	.0495	40	64	.00491	0	-6	14.60
									1	-3	14.65
									2	0	14.70
									3	0	14.70
									4	0	14.70
									5	0	14.70
									6	0	14.70
									7	0	14.70

APPENDIX C: REATTACHMENT "ZERO ZONE" DATA

RUN #	PROBE	P_1 (PSIA)	T_1 (°F)	$\triangle P$ (PSI)	$\dot{m}$ (LBM/SEC)	P_B (PSIA)	T_B (°F)	$\dot{m}_B$ (LBM/SEC)	STA (IN)	P_S (MV)	P_S (PSIA)
Z11	PITOT	130	216	1.35	.0655				0	-18	14.41
									1	-10	14.54
									2	-4	14.64
									3	-1	14.68
									4	0	14.70
									5	0	14.70
									6	0	14.70
									7	0	14.70
Z12	PITOT	130.5	214	1.45	.0653	56	63	.00688	0	-14	14.48
									1	-7	14.59
									2	-1	14.68
									3	0	14.70
									4	1	14.72
									5	1	14.72
									6	1	14.72
									7	0	14.70
Z13	PITOT	132	221	2.93	.0966				0	-36	14.12
									1	-21	14.36
									2	-9	14.56
									3	-4	14.64
									4	0	14.70
									5	0	14.70
									6	0	14.70
									7	0	14.70

APPENDIX C: REATTACHMENT "ZERO ZONE" DATA

RUN #	PROBE	P_1 (PSIA)	T_1 (°F)	$\triangle P$ (PSI)	$\dot{m}$ (LBM/SEC)	P_B (PSIA)	T_B (°F)	$\dot{m}_B$ (LBM/SEC)	STA (IN)	P_S (MV)	P_S (PSIA)
Z14	PITOT	130.5	218	2.93	.0962	80	62	.00984	0	-30	14.22
									1	-15	14.46
									2	-5	14.62
									3	0	14.70
									4	2	14.73
									5	1	14.72
									6	1	14.72
									7	0	14.70
Z15	PITOT	130.5	212	6.63	.1442				0	-83	13.37
									1	-54	13.84
									2	-25	14.30
									3	-13	14.49
									4	-3	14.65
									5	-1	14.68
									6	0	14.70
									7	-1	14.68
Z16	PITOT	130.5	220	6.63	.1433	95	61	.0112	0	-74	13.52
									1	-45	13.98
									2	-18	14.41
									3	-6	14.60
									4	0	14.70
									5	0	14.70
									6	2	14.73
									7	-1	14.68

Appendix D Hot Wire Calibration Data

A hot wire was used for the mass fraction analysis. As previously described (Ref. 7), sonic choked flow nozzles were used for controlling and measuring the flow rate of the air and helium for the calibration of this hot wire. Changes in the percentage helium in the mixture were detected by the hot wire inserted in the gas sampling tank and recorded as changes in DC voltage through the TSI calibration instrument.

P_{air} (PSIA)	T_{air} (°F)	P_{He} (PSIA)	T_{He} (°F)	E (VOLTS)	$\dot{m}_{air}$ (LBM/SEC)	$\dot{m}_{He}$ (LBM/SEC)	%He
216.7	73	0		1.521	8.25×10^{-4}	0	0
213.2	73	40.1	73	1.975	8.12×10^{-4}	1.14×10^{-4}	12.3
215.7	73	54.4	73	2.062	8.21×10^{-4}	1.55×10^{-4}	15.9
214.7	73	76.7	73	2.160	8.17×10^{-4}	2.18×10^{-4}	21.1
213.7	73	114.7	73	2.267	8.14×10^{-4}	3.26×10^{-4}	28.6
213.2	73	140.7	73	2.316	8.12×10^{-4}	4.00×10^{-4}	33.0
212.7	73	182.7	73	2.373	8.10×10^{-4}	5.19×10^{-4}	39.1
136.7	73	168.7	73	2.439	5.21×10^{-4}	4.79×10^{-4}	47.9
56.2	73	123.7	73	2.520	2.14×10^{-4}	3.52×10^{-4}	62.2
0		113.2	73	2.638	0	3.22×10^{-4}	100.0

Appendix E

Mass Fraction Analysis

Calibration Curve

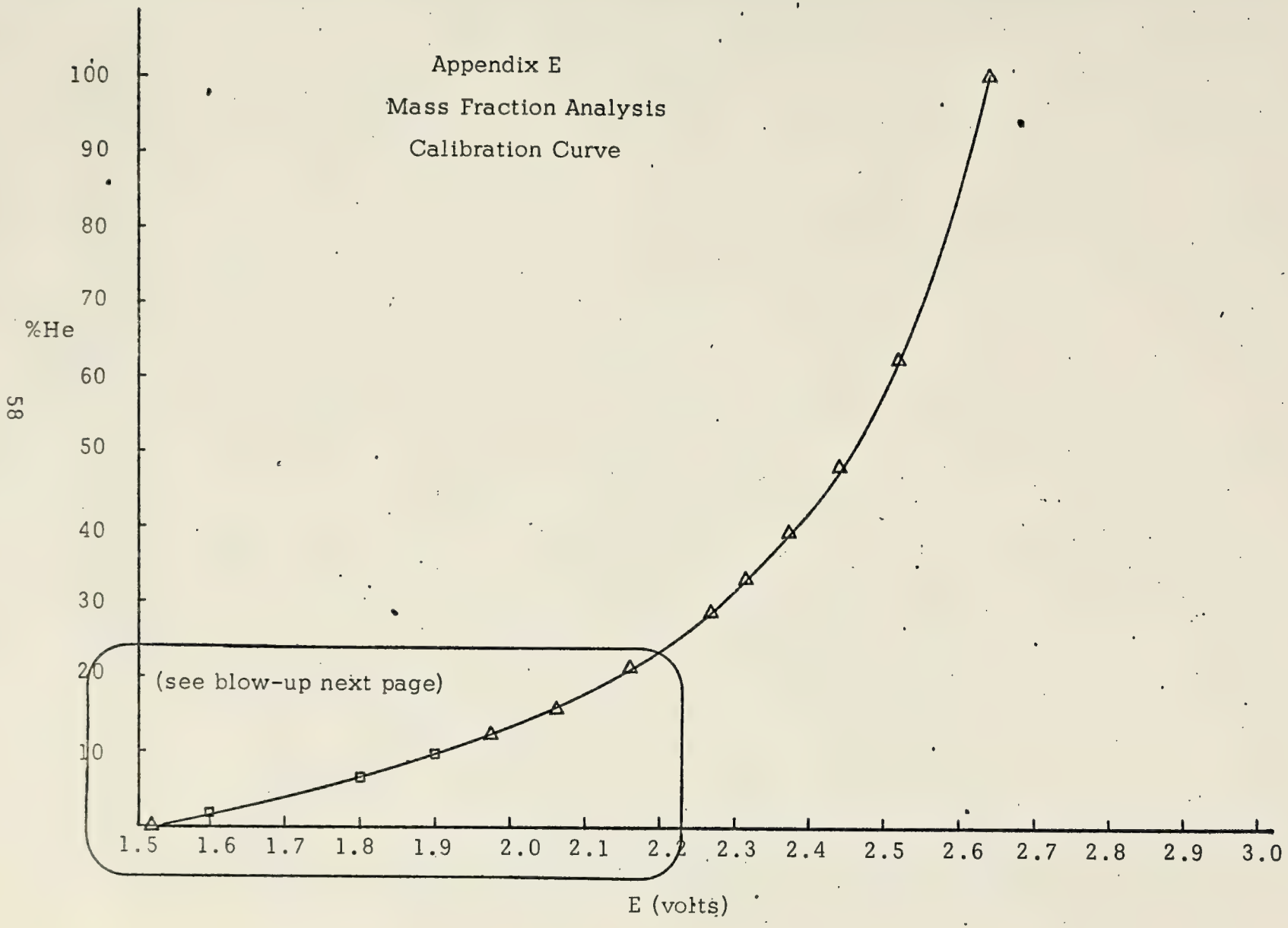

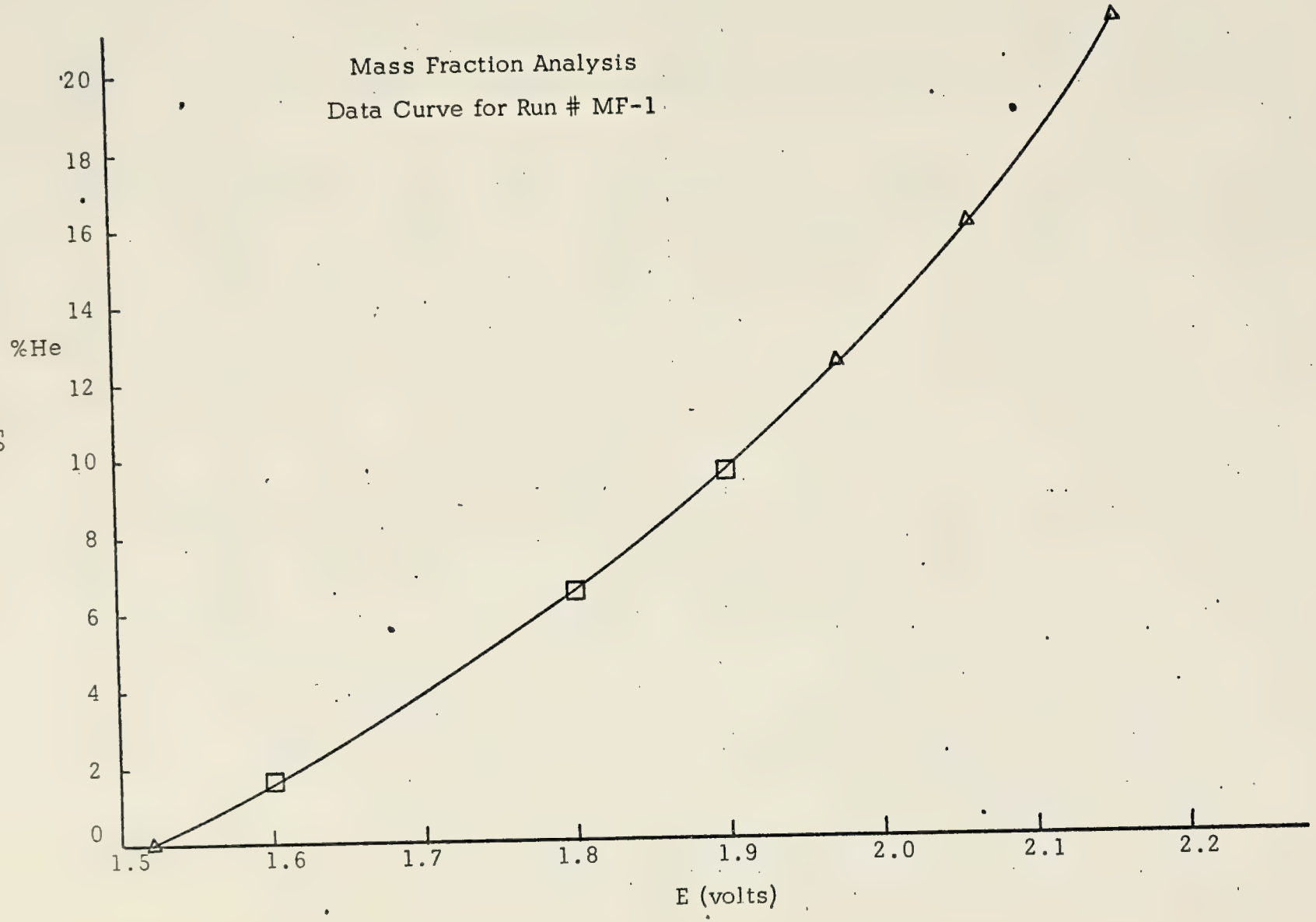
Mass Fraction Analysis
Data Curve for Run # MF-1
%He
20
18
16
14
12
10
8
6
4
2
0
1.5
1.6
1.7
1.8
1.9
2.0
2.1
2.2
E (volts)

APPENDIX E: MASS FRACTION ANALYSIS DATA

Run #	P_1	T_1	ΔP	$\dot{m}$	P_B	T_B	$\dot{m}_B$
MF-1	130.5 psia	58°F	.60 psi	.0501 lbm/sec	35 psia	65°F	.00511 lbm/sec

Station	6 INCHES		5 INCHES		4 INCHES		3 INCHES		2 INCHES		1 INCH	
	E_{DC} (VOLTS)	%He	E_{DC} (VOLTS)	%He	E_{DC} (VOLTS)	%He	E_{DC} (VOLTS)	%He	E_{DC} (VOLTS)	%He	E_{DC} (VOLTS)	%He
1	2.080	16.7			2.017	13.9	2.048	15.3				
2	1.931	10.7			1.914	10.0	1.952	11.4				
3	1.856	8.1			1.845	7.8	1.892	9.3				
4	1.812	6.8			1.780	5.9	1.805	6.7				
5	1.796	6.4			1.736	4.8	1.677	3.3				
6	1.787	6.1			1.732	4.7	1.705	4.0				
7	1.959	11.7			1.847	7.8	1.827	7.3				

HIGHLY TURBULENT RECIRCULATION ZONE (MAY APPROACH A WELL-STIRRED REACTOR)

DIFFUSION FLAME LOCATED IN TURBULENT BOUNDARY LAYER WITH HIGH DEGREE OF OXIDIZER DILUTION

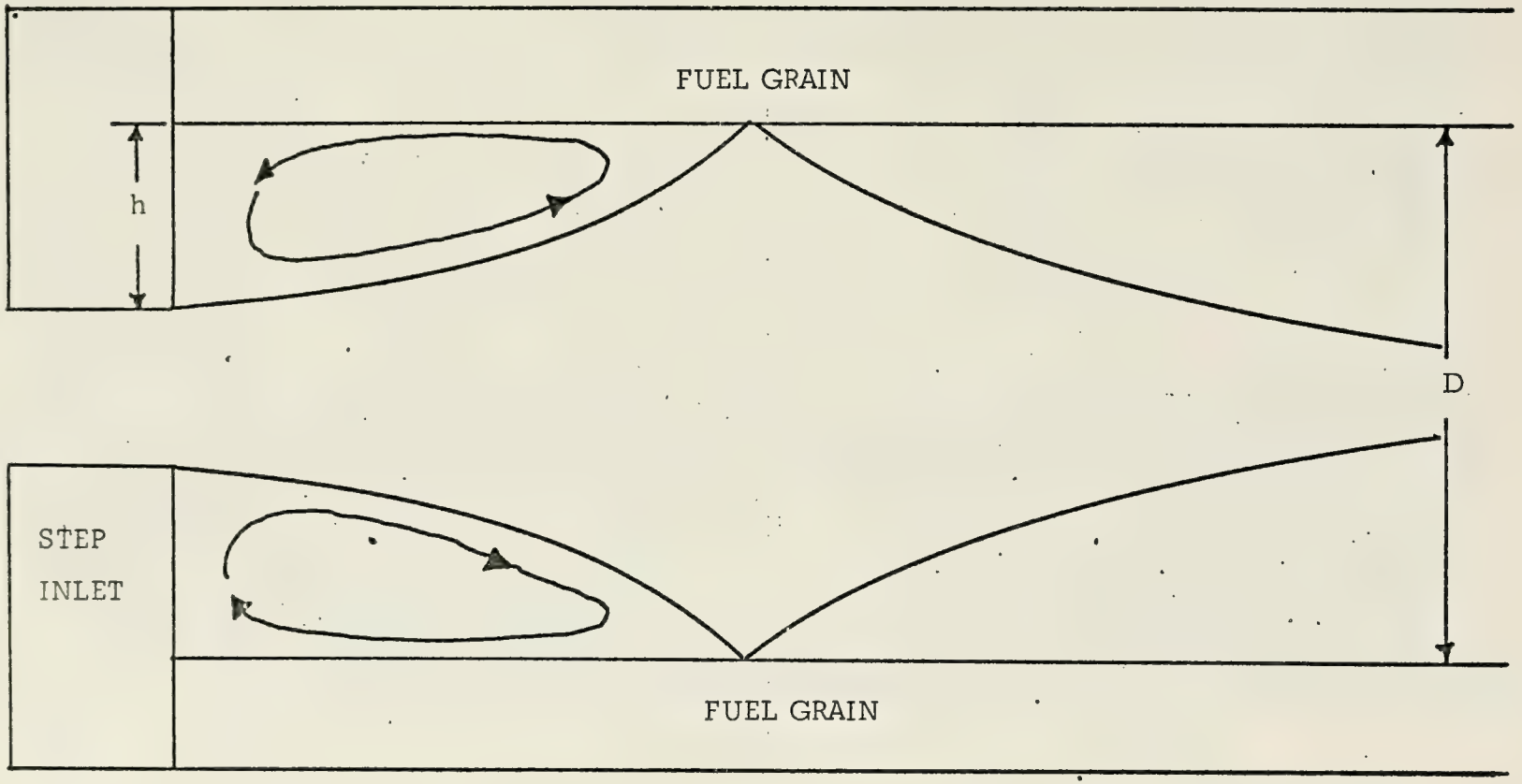

Figure 1. Combustion Mechanisms

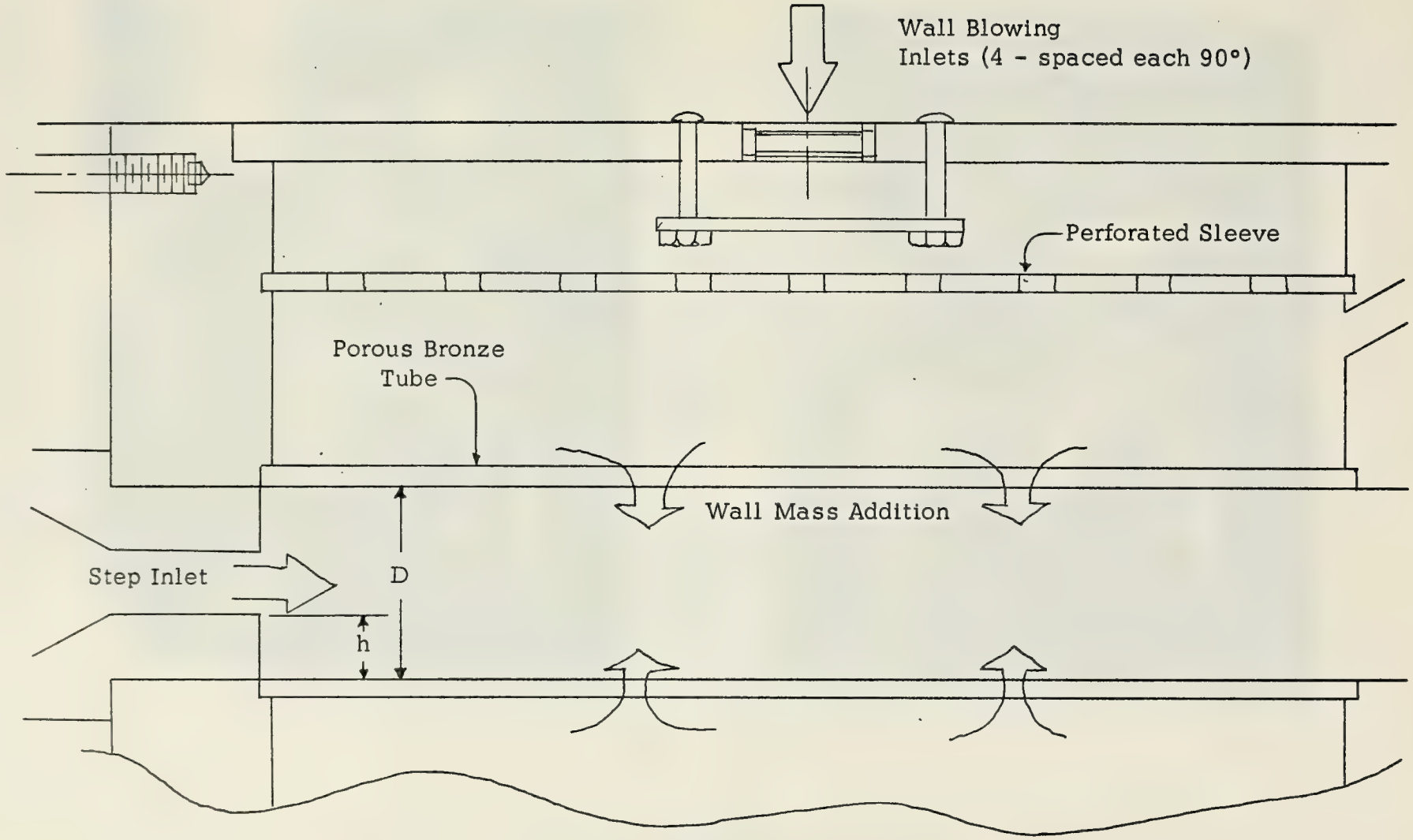

Figure 2. Schematic of ramjet model

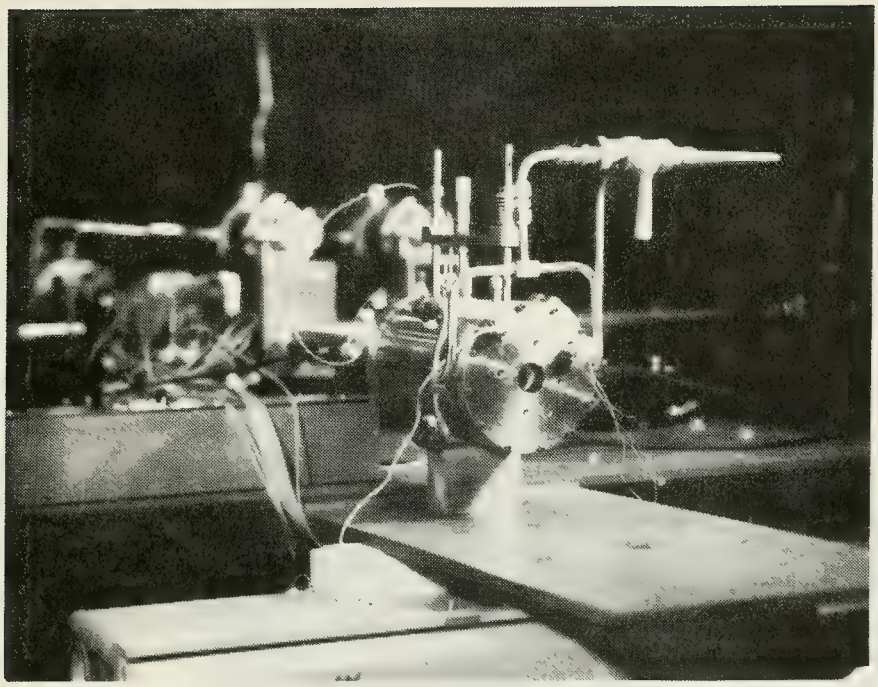

Figure 3. Ramjet Model Installed in Test Cell

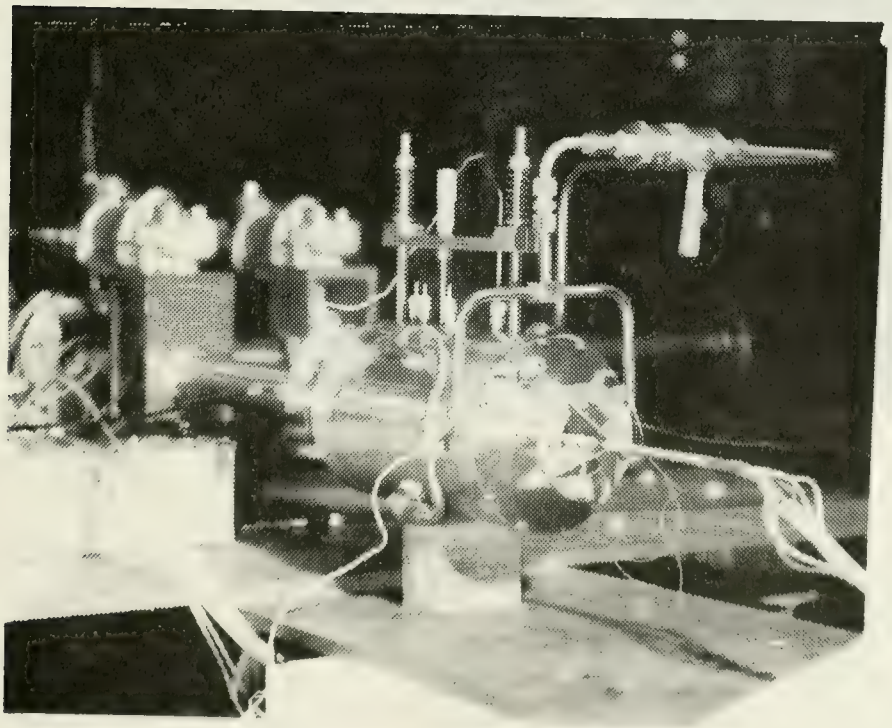

Figure 4. Ramjet Model with Pressure Probe Installed

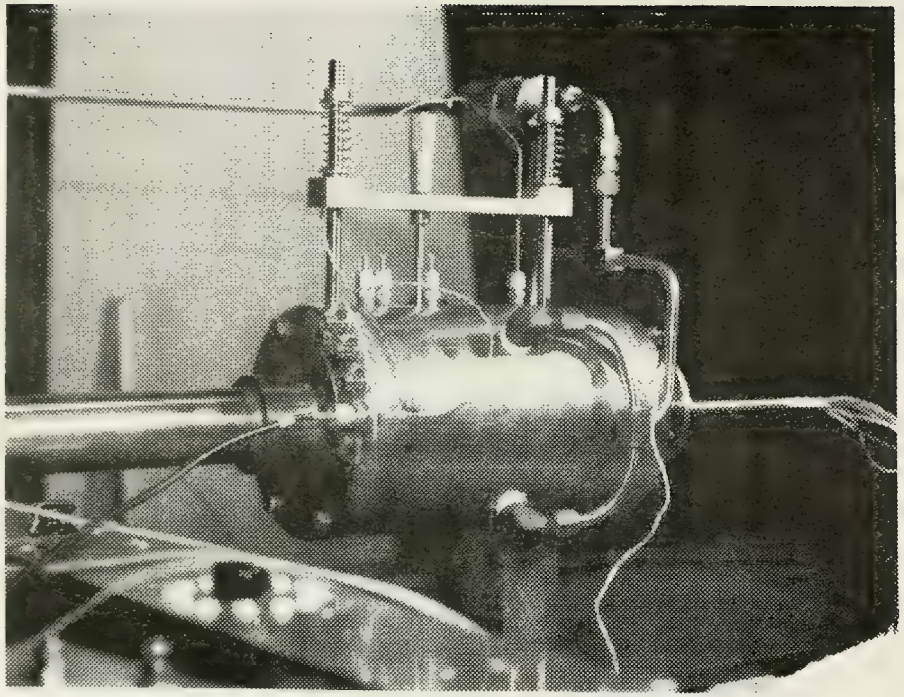

Figure 5. Detail of Hot Wire Traverse Apparatus

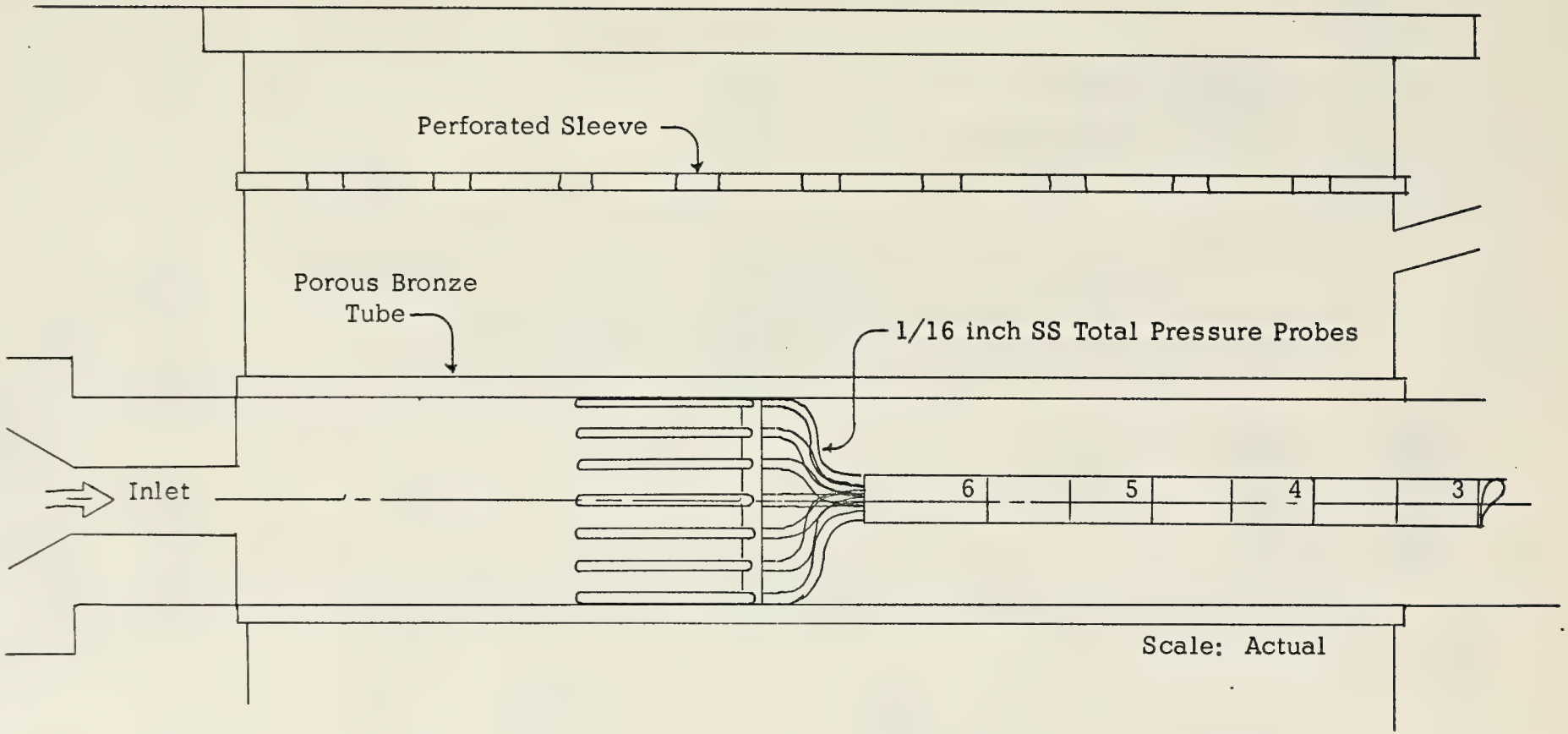

Figure 6. Total Pressure Rake - Installed

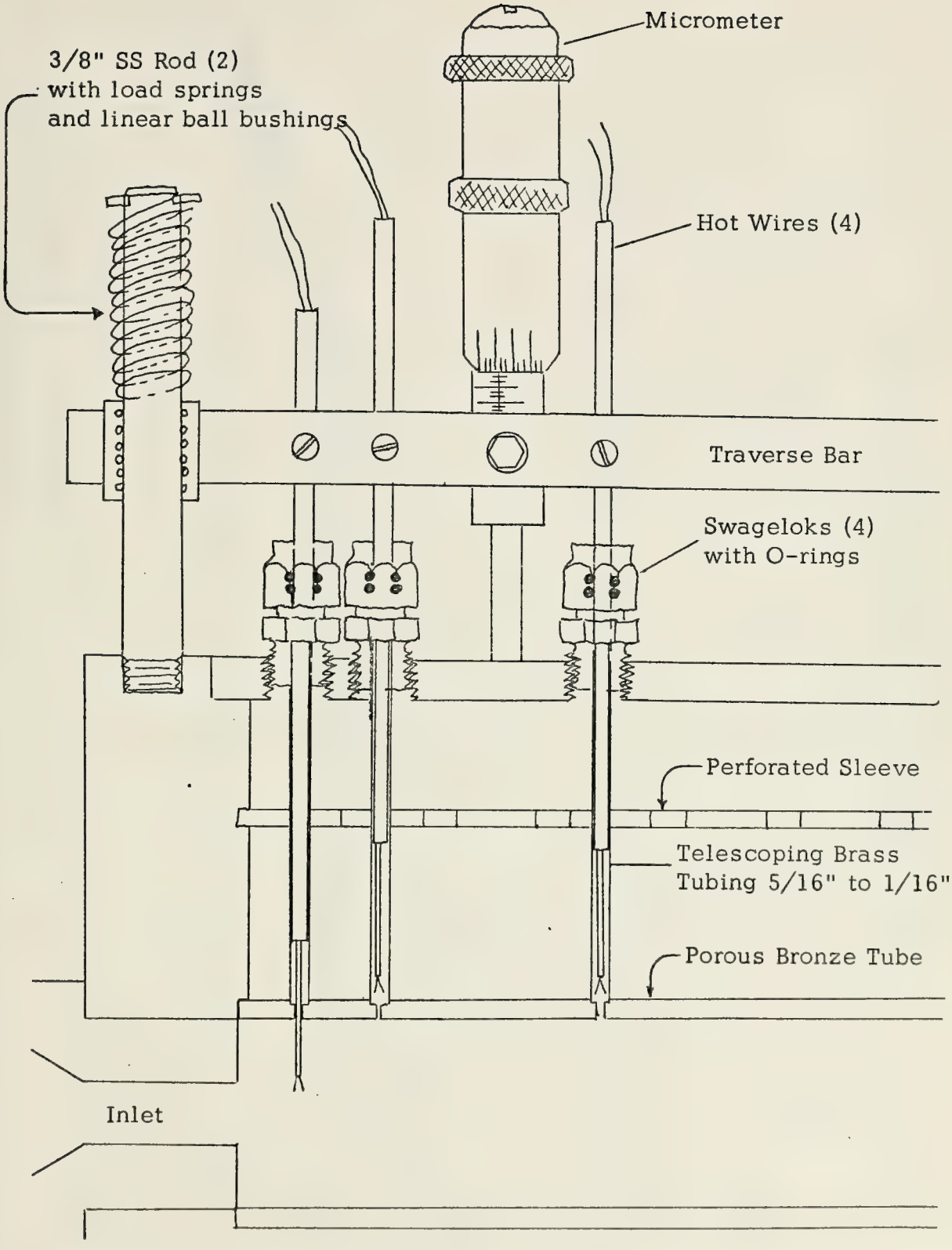

Figure 7. Schematic of Hot Wire Installation and Traverse

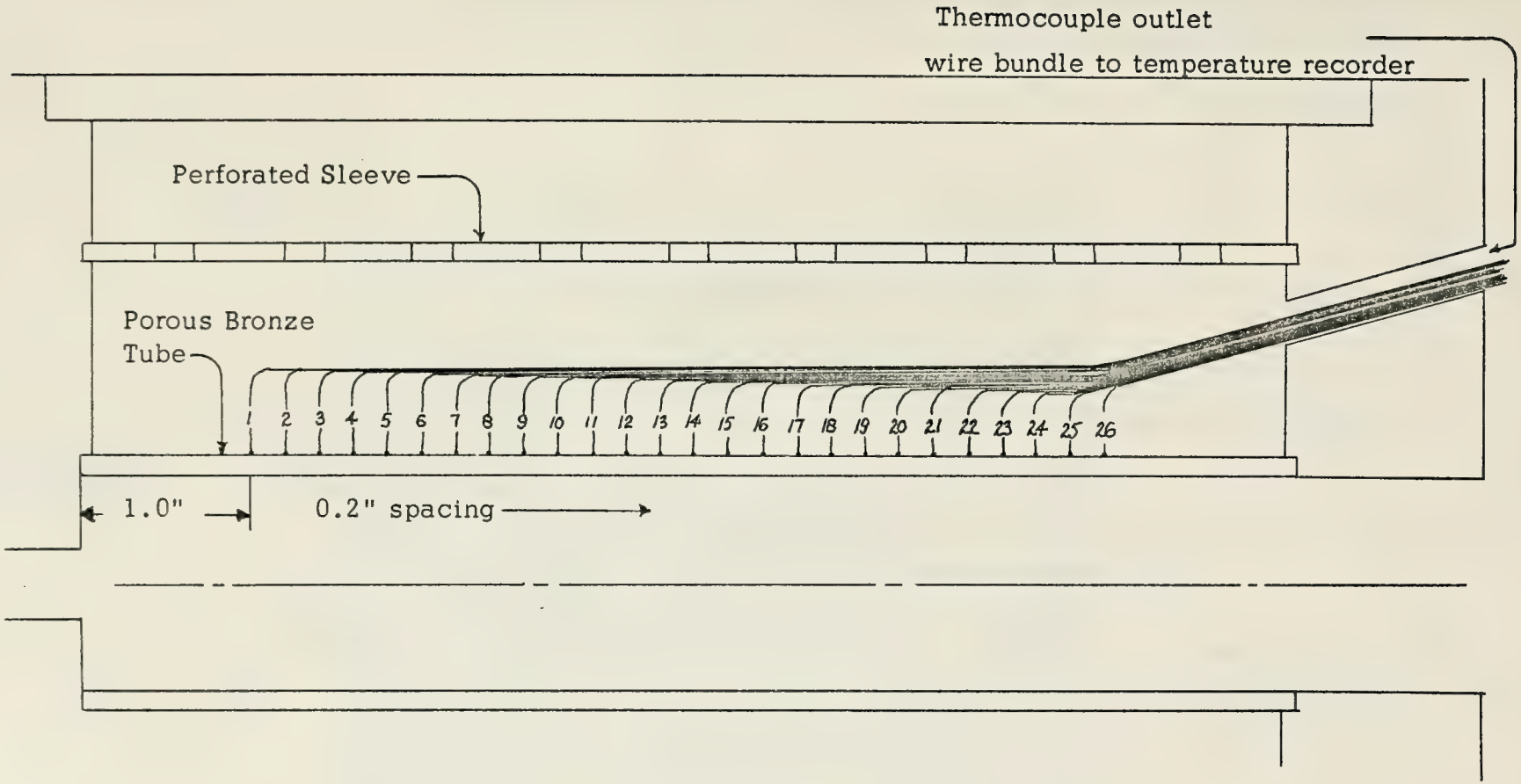

Figure 8. Schematic of Thermocouple Connections

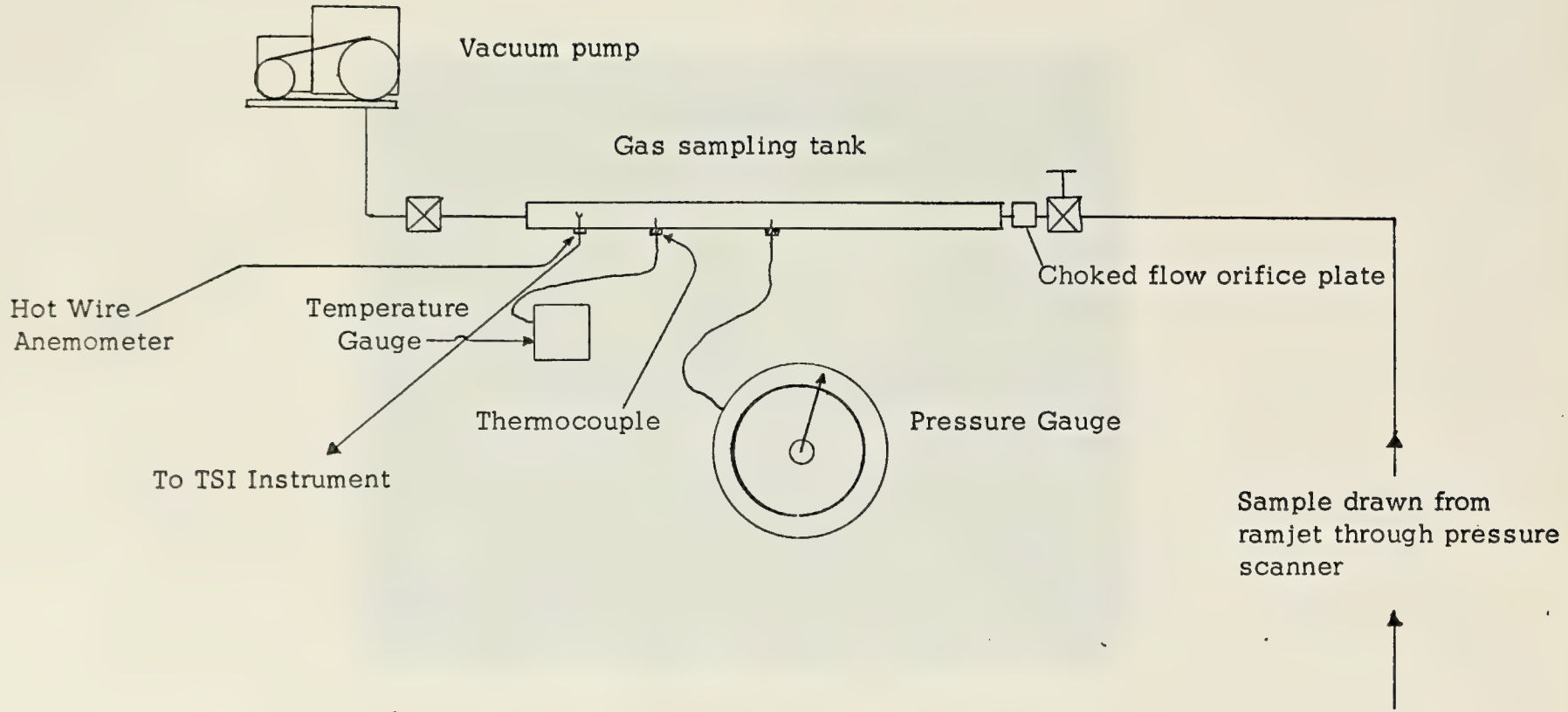

Figure 9. Schematic of Mass Fraction Analysis Apparatus

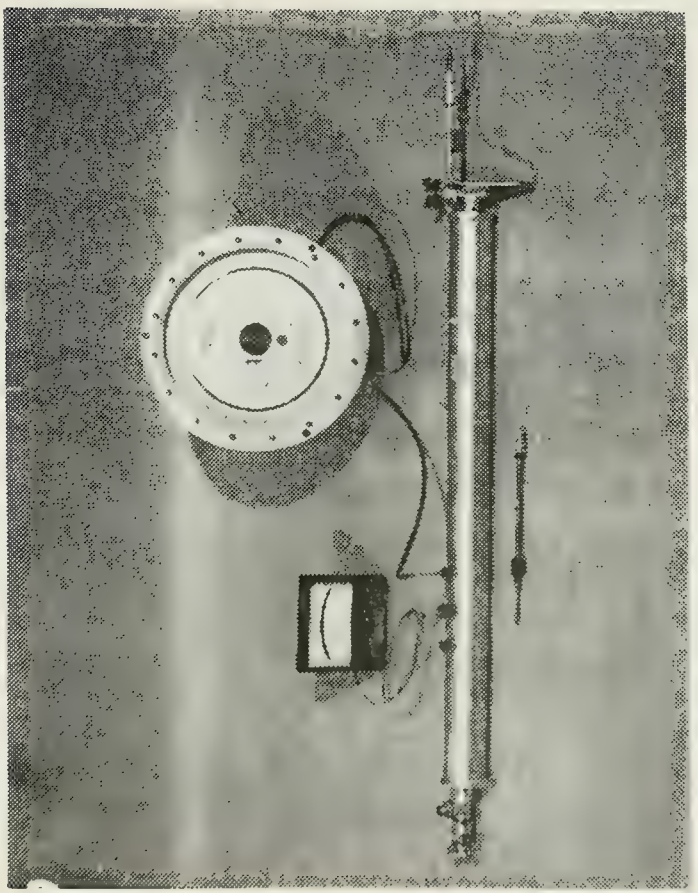

Figure 10. Mass Fraction Analysis Apparatus

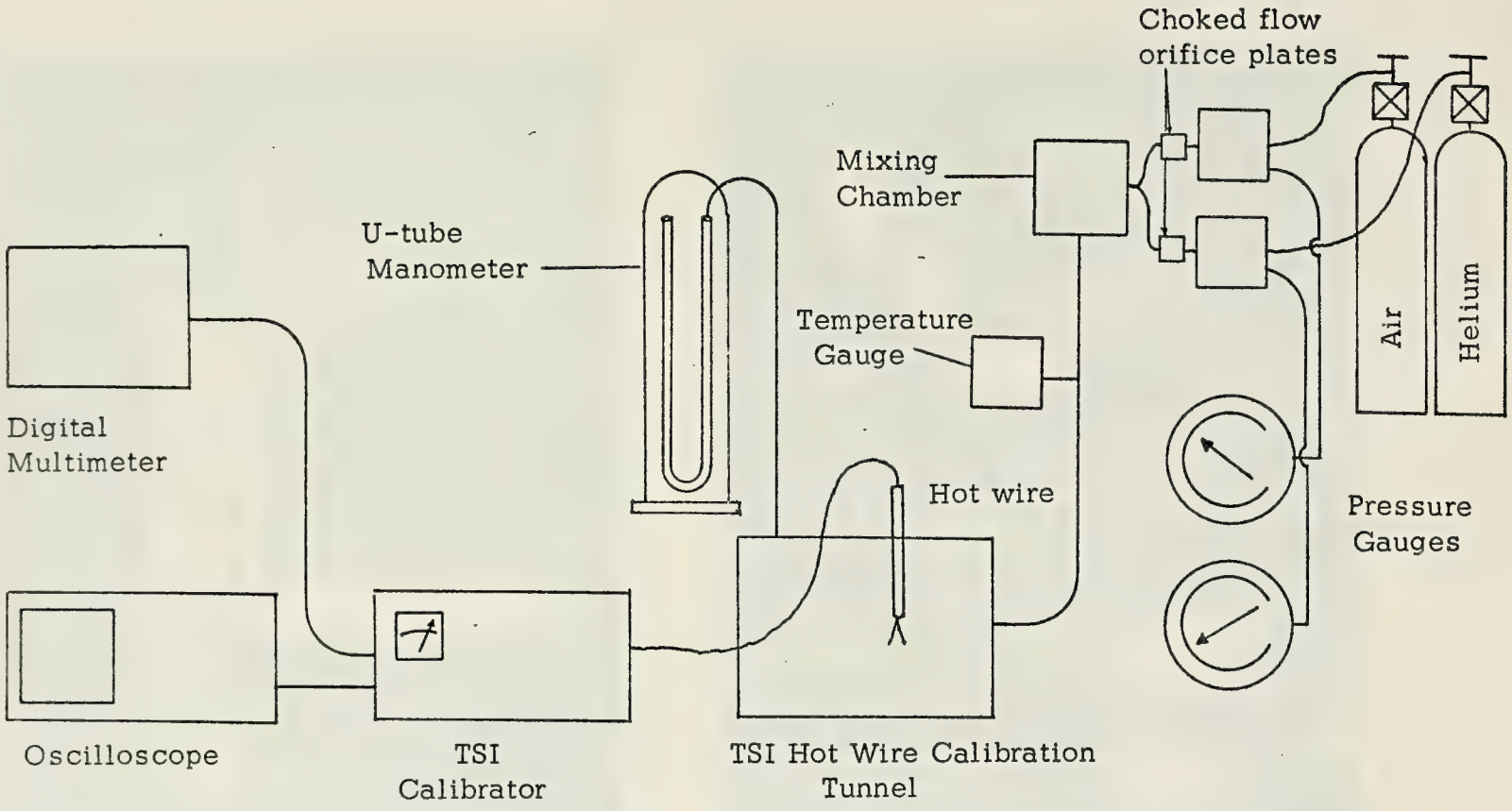

Figure 11. Schematic of Mass Fraction Hot Wire Calibration Apparatus

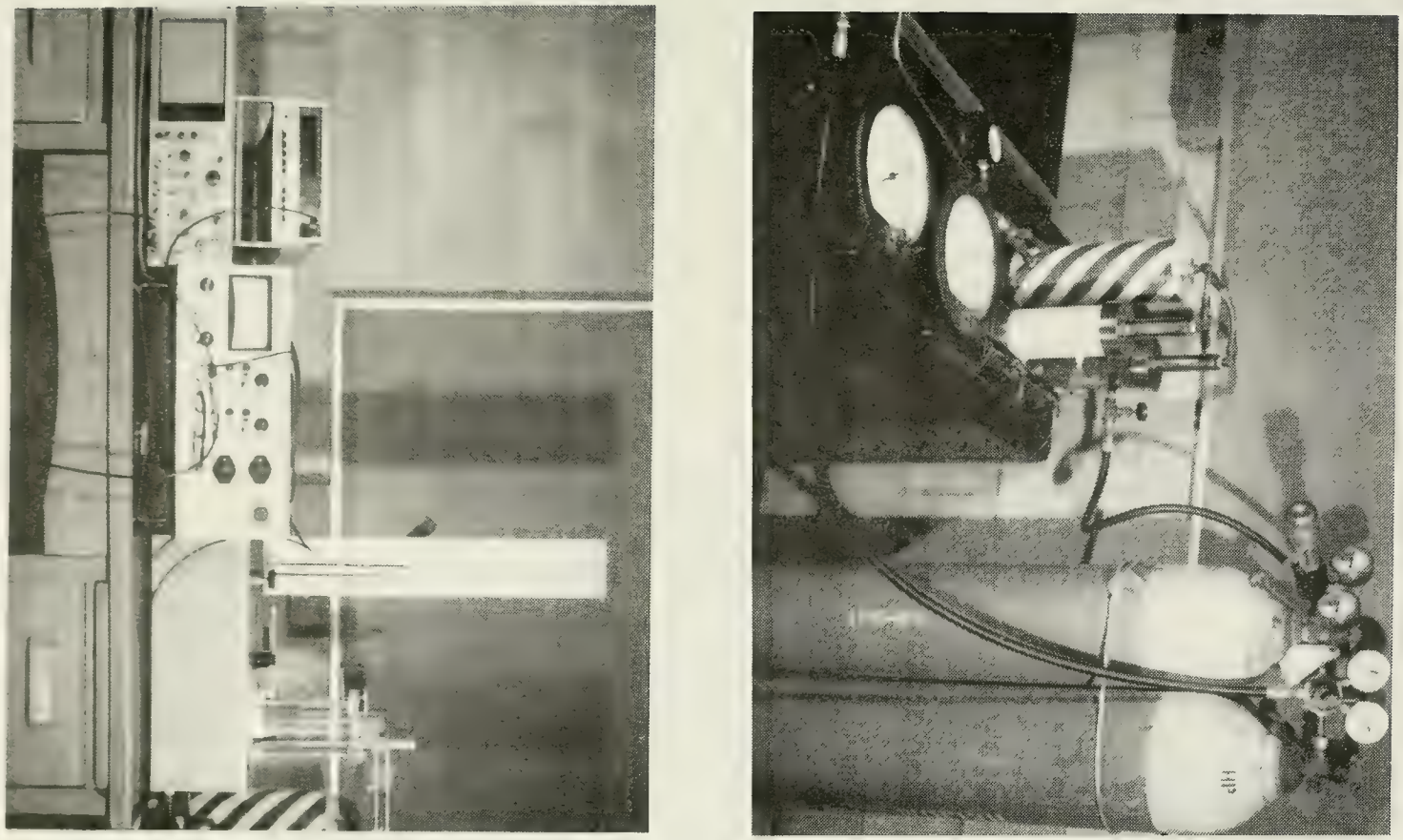

Figure 12. Mass Fraction Hot Wire Calibration Apparatus

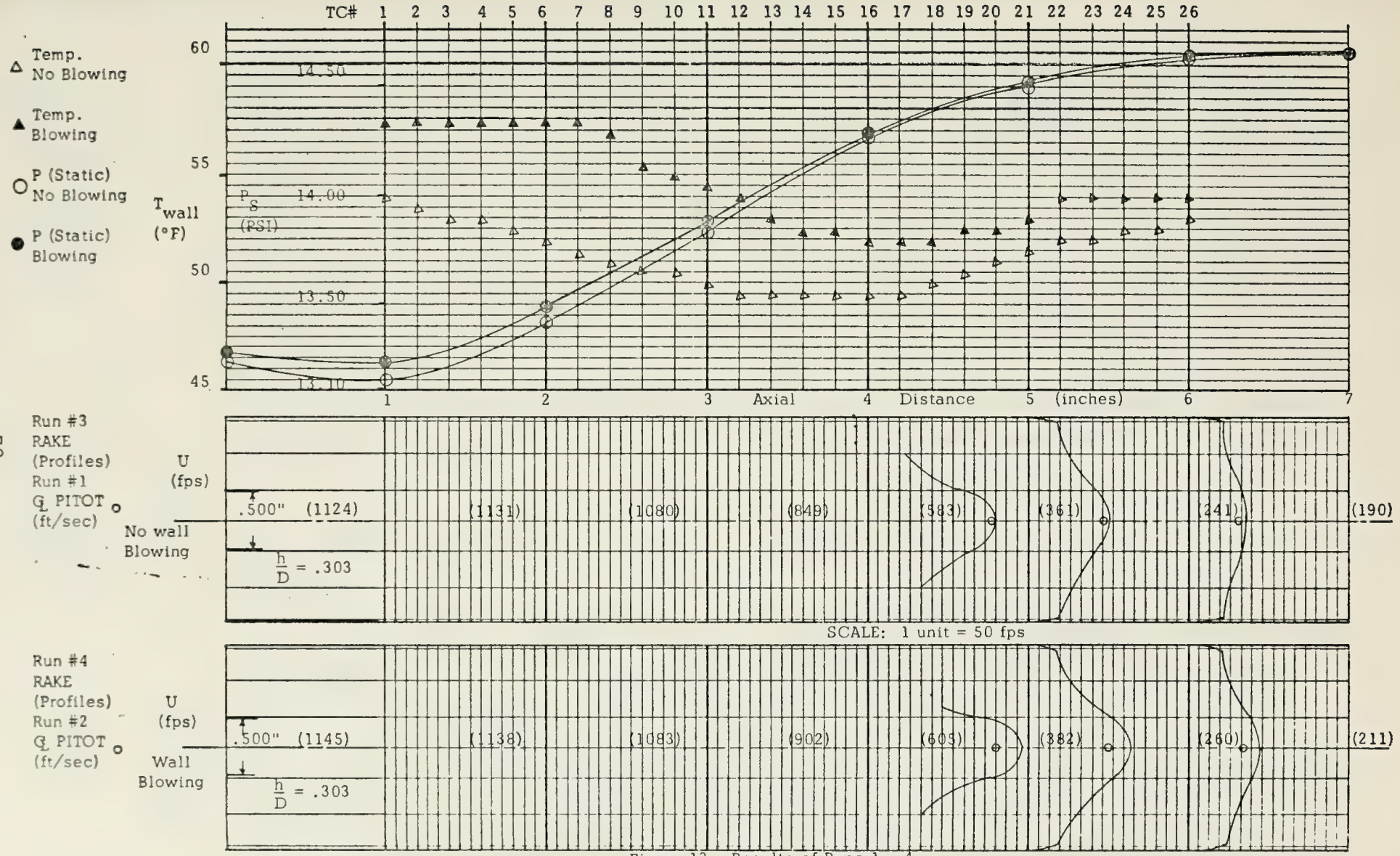

Figure 13. Results of Runs 1 - 4

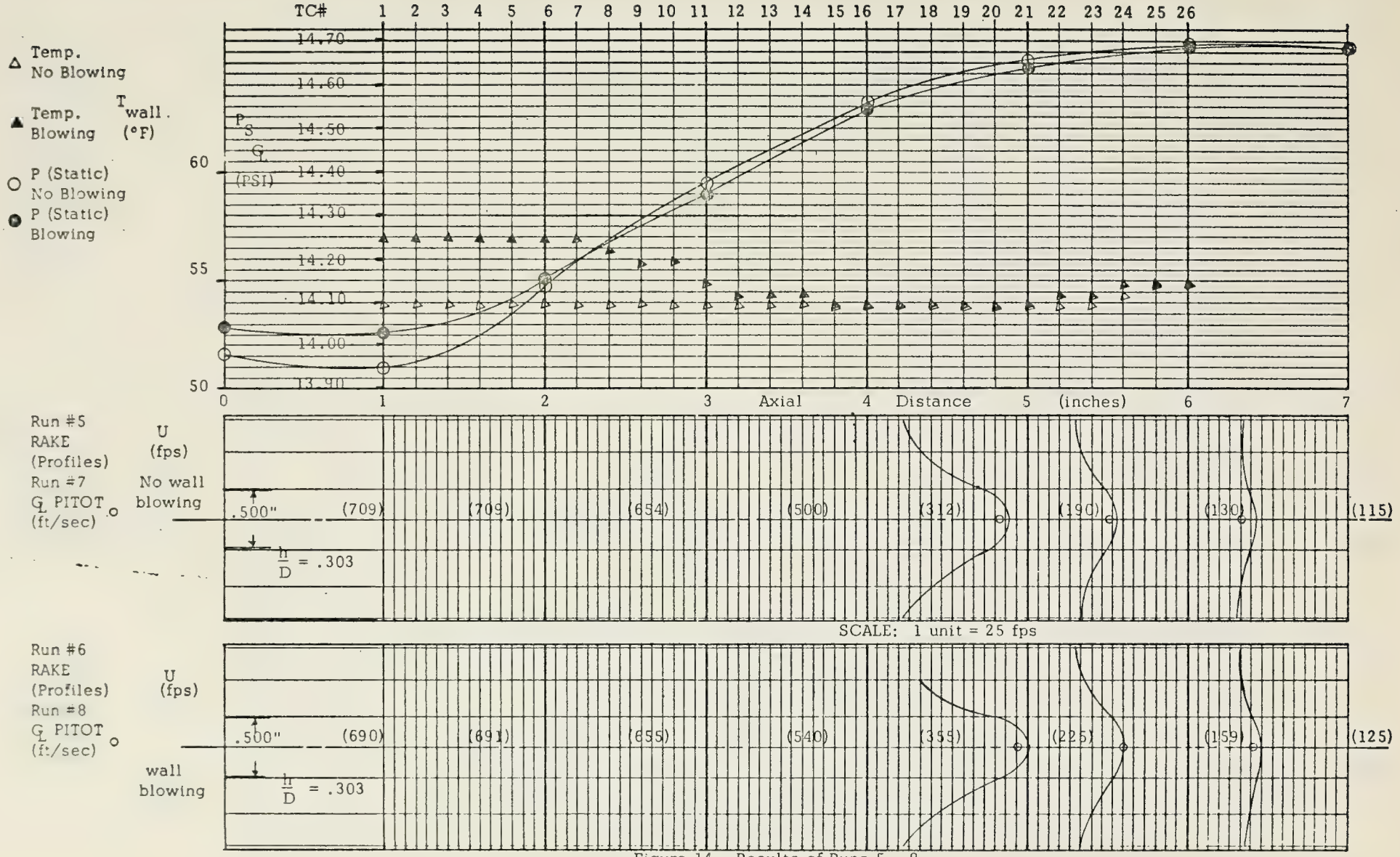

Figure 14. Results of Runs 5 - 8

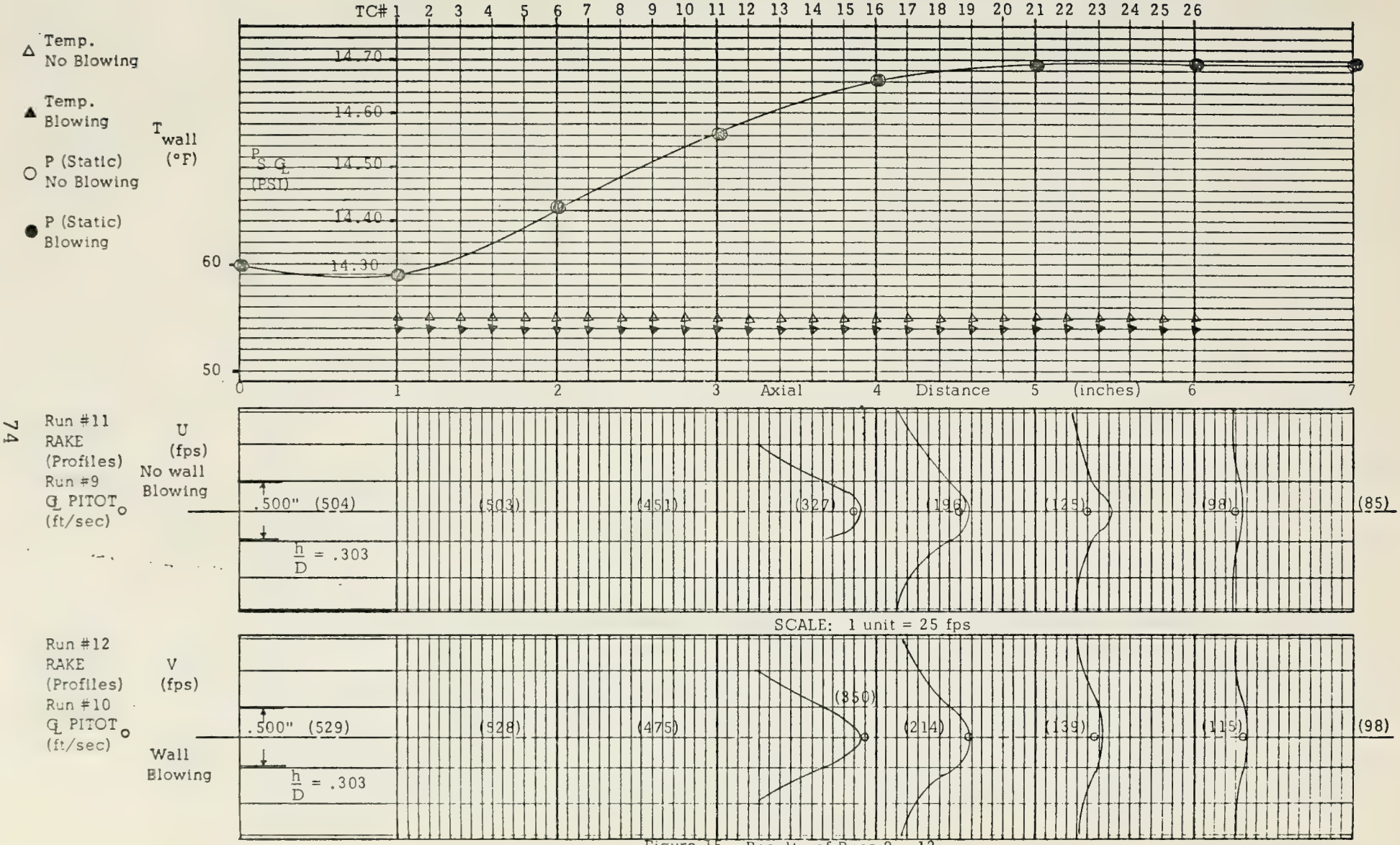

Figure 15. Results of Runs 9 - 12

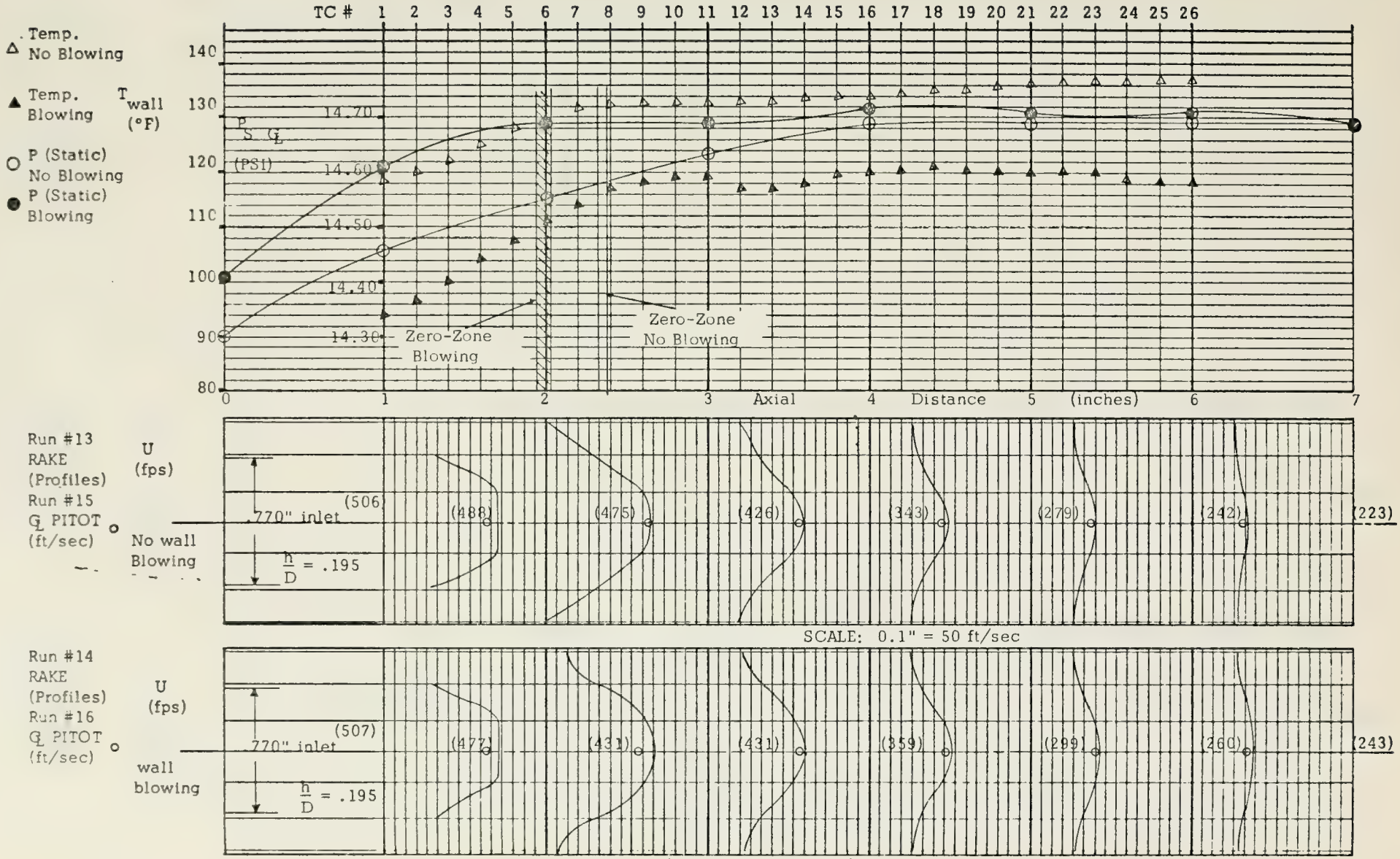

Figure 16. Results of Runs 13 - 16

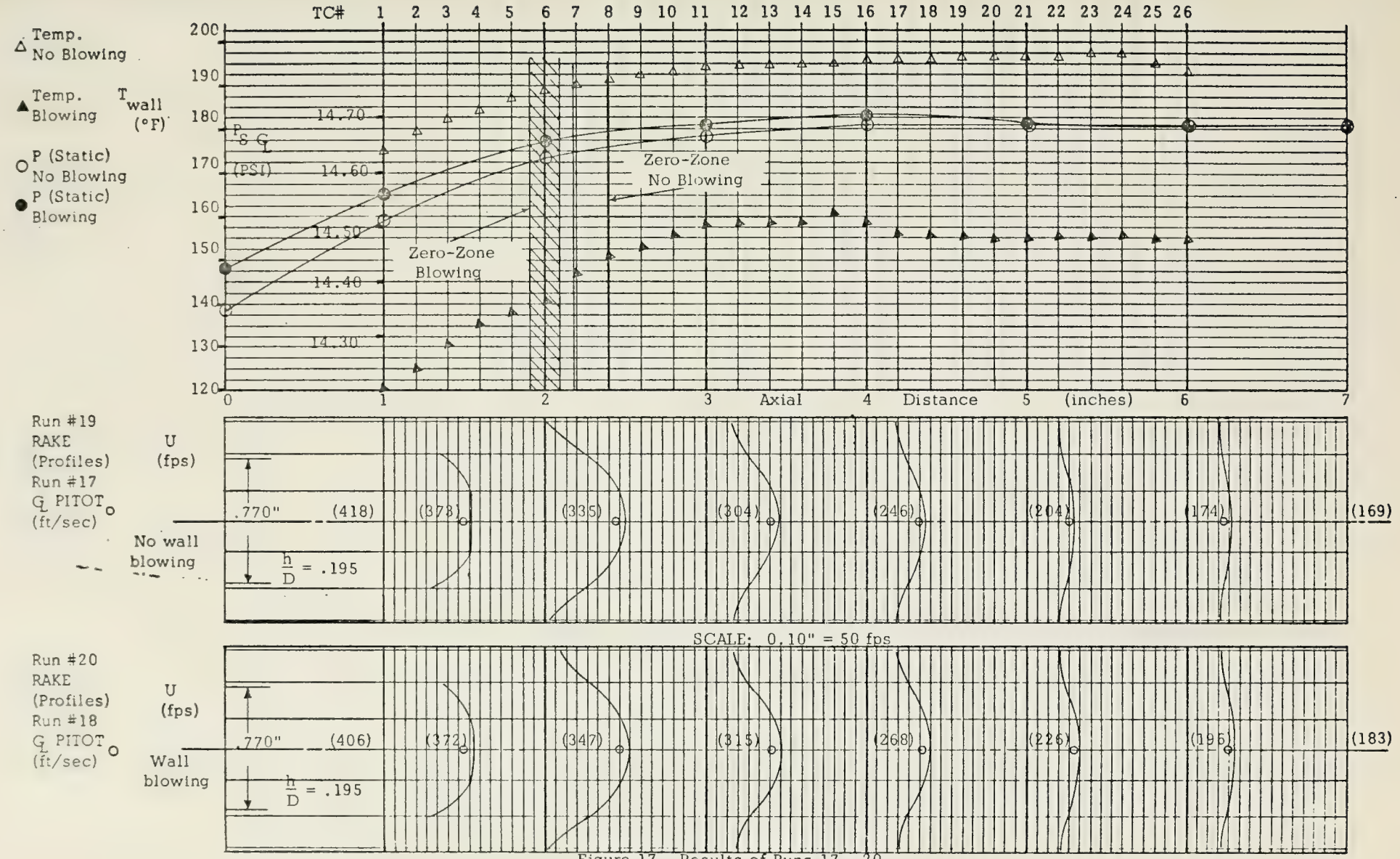

Figure 17. Results of Runs 17 - 20

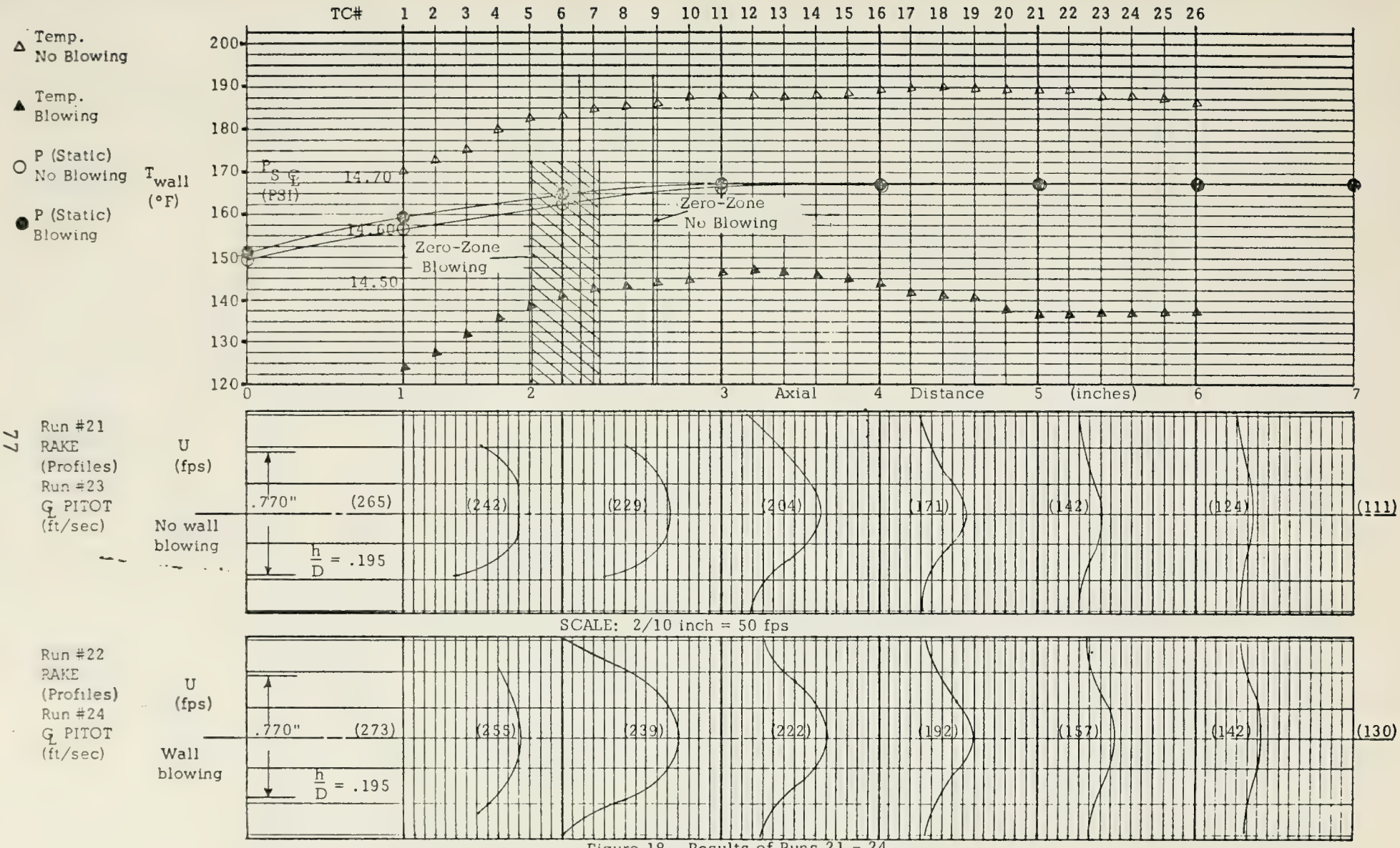

Figure 18. Results of Runs 21 - 24

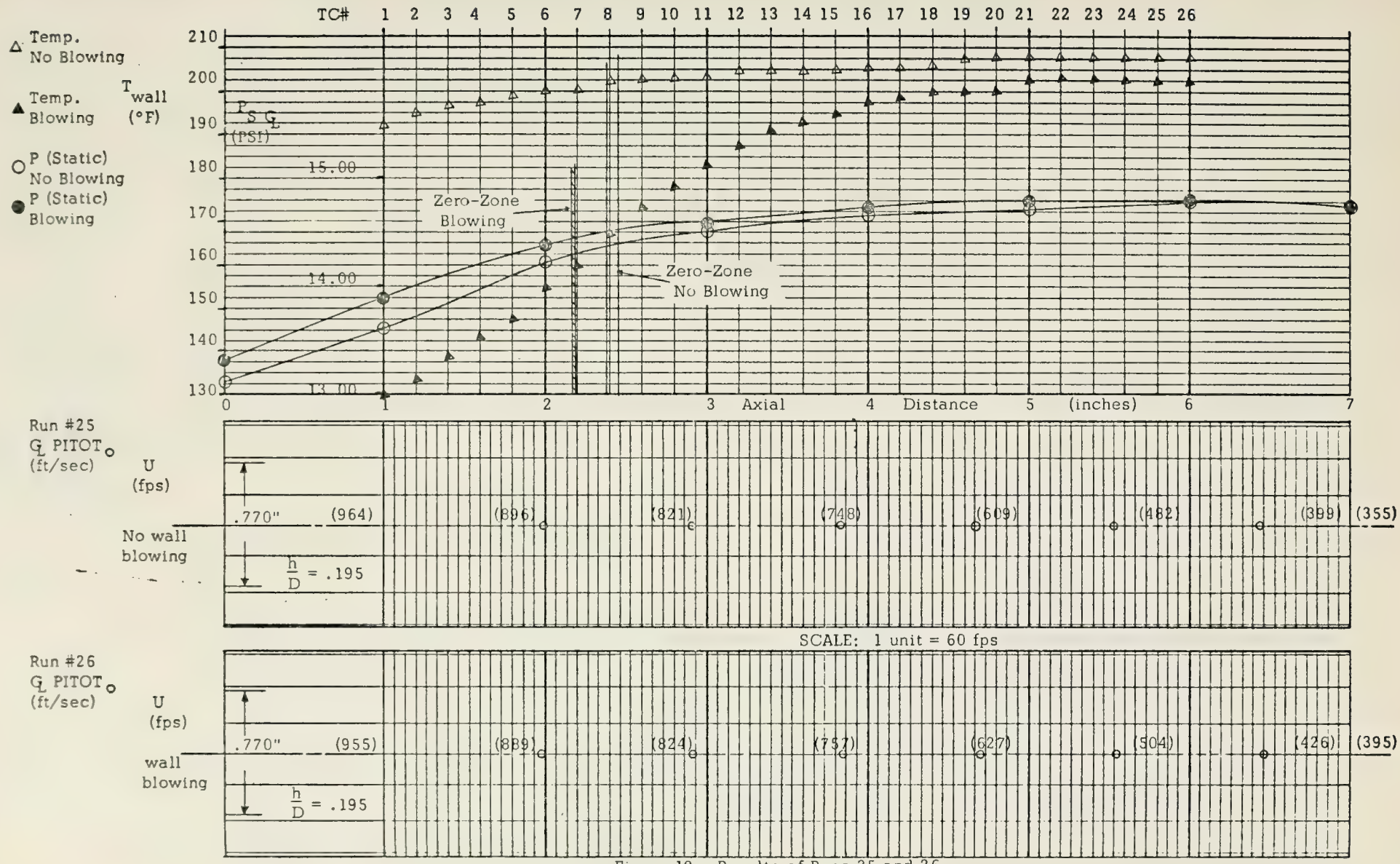

Figure 19. Results of Runs 25 and 26

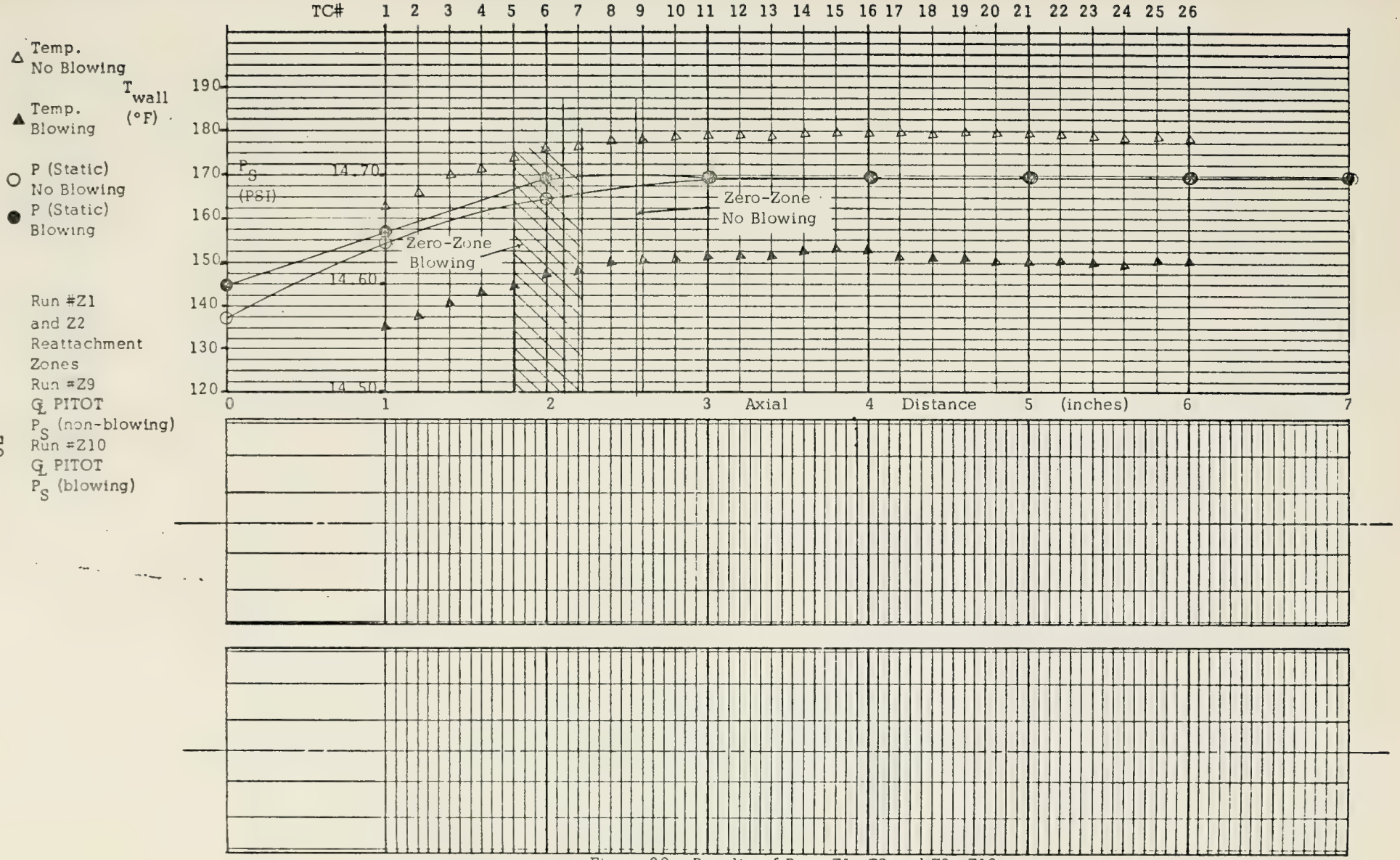

Figure 20. Results of Runs Z1, Z2 and Z9, Z10

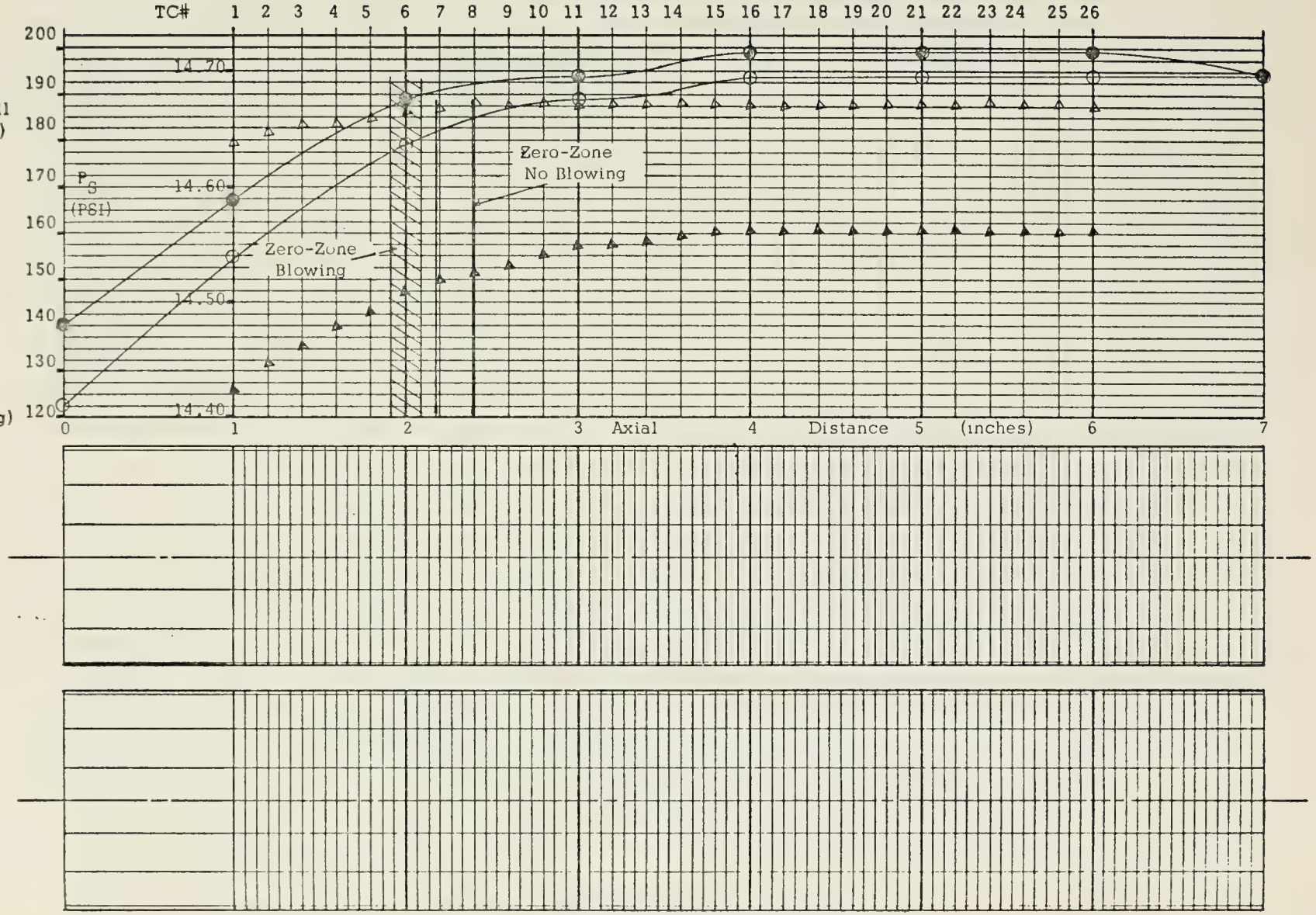

Figure 21. Results of Runs Z3, Z4, Z11 and Z12

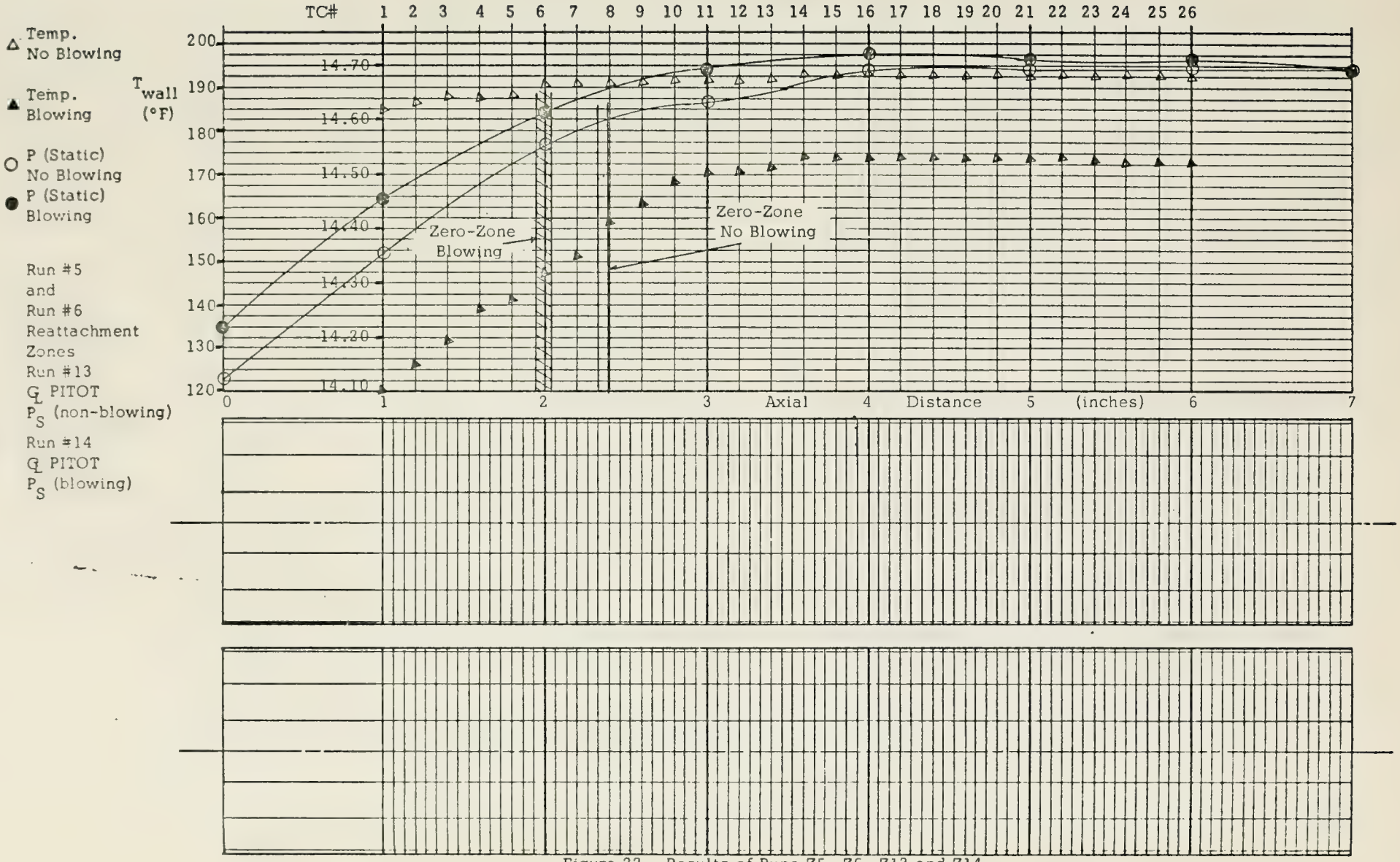

Figure 22. Results of Runs Z5, Z6, Z13 and Z14

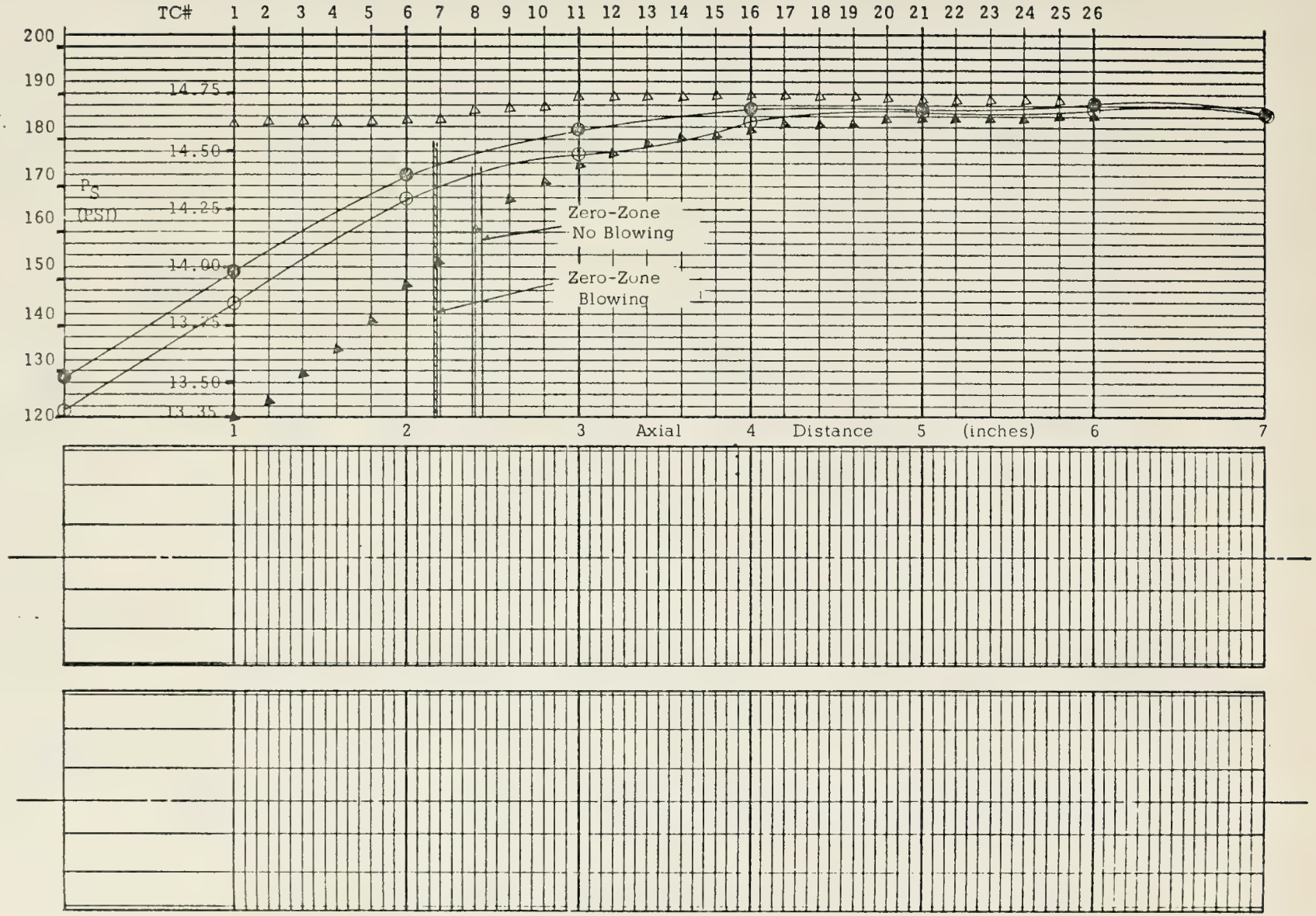

Figure 23. Results of Runs Z7, Z8, Z15 and Z16

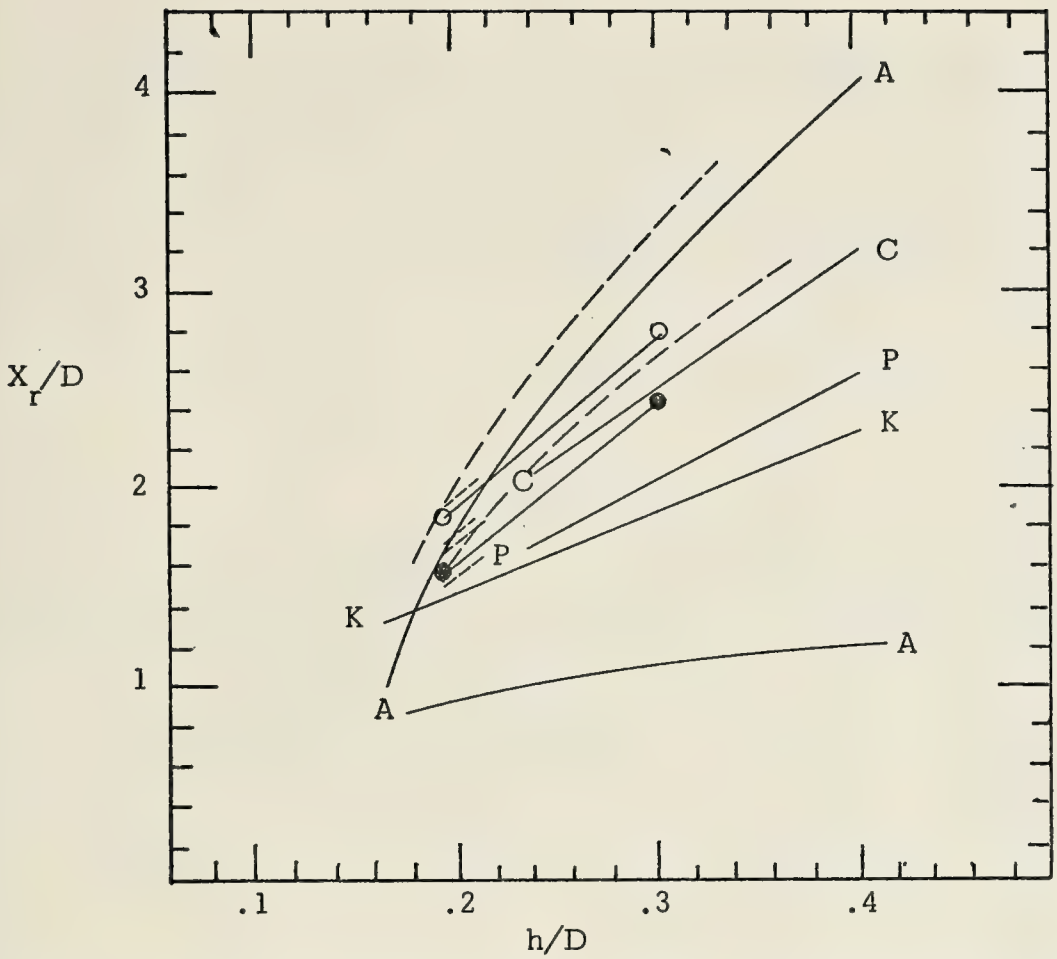

K-K Krall and Sparrow - based on location of maximum heat transfer coefficient (axisymmetric flow)

A-A Abbott and Kline - note different reattachment point locations for each side of 2-D channel and spread-out zone

P-P PISTEP II results

C-C Boaz and Netzer results

Present Investigation - no wall mass addition

Present Investigation - with 10% wall mass addition showing spread-out region at h/D = .195

Figure 24. Reattachment Point Data Comparison

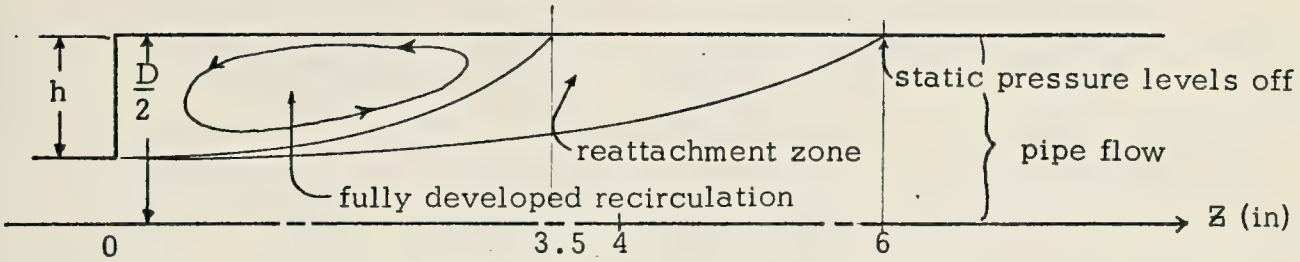

Figure 25. Typical Reattachment Zone - Large Step

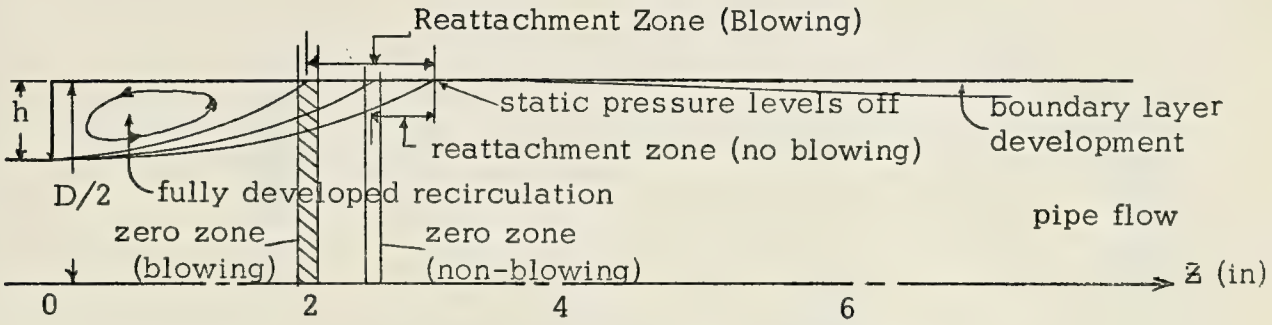

Figure 26. Typical Reattachment Zone - Small Step

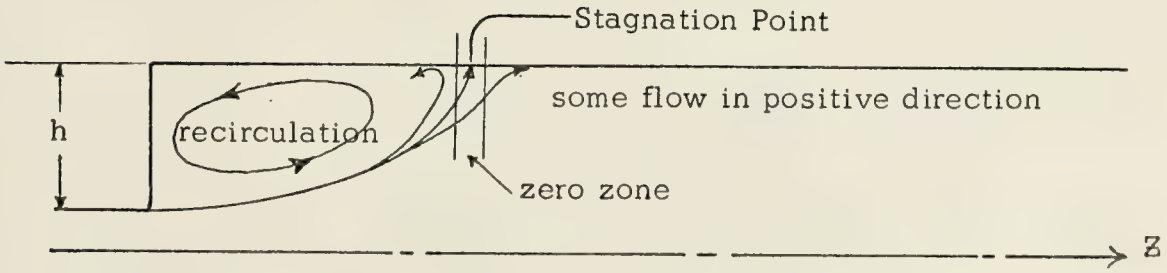

Figure 27. "Zero Zone" Leading Edge of Flow Reattachment

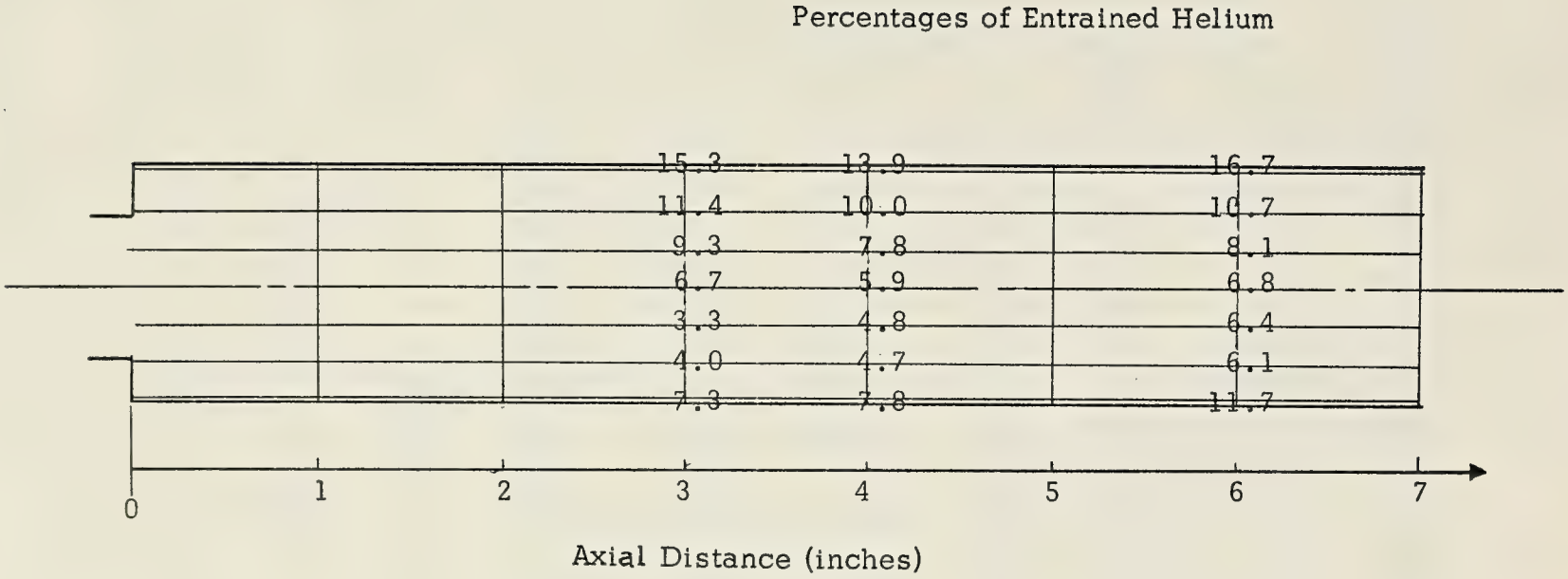

Figure 28. Mass Fraction Distribution

LIST OF REFERENCES

1. Iwanciow, B.L., Hulzman, A.L., Dunlap, R., "Combustion Stabilization in a Solid Fuel Ramjet," 10th JANNAF Combustion Meeting, CPIA Publication 243, Vol. III, pp. 197-214, December, 1973.

2. Abbott, D.E. and Kline, J. S., "Experimental Investigation of Subsonic Turbulent Flow Over Single and Double Backward Facing Steps," Journal of Basic Engineering, p. 317, September 1962.

3. Krall, K. M. and Sparrow, E. M., "Turbulent Heat Transfer in Separated, Reattached, and Redevelopment Regions of a Circular Tube," Journal of Heat Transfer, p. 131, February 1966.

4. Naval Postgraduate School Report 57NT73031A, An Investigation Of The Internal Ballistics Of Solid Fuel Ramjets, by L. D. Boaz and D. W. Netzer, 1 March 1973.

5. Naval Postgraduate School Report 57NT73091B, An Investigation Of The Internal Ballistics of Solid Fuel Ramjets - A Progress Report, by L. D. Boaz, C. E. Jones, III, and D. W. Netzer, September 1973.

6. Flow Measurement - Supplement to Power Test Codes, v. 19.5;4, The American Society of Mechanical Engineers, 1959.

7. John, James E. A., Gas Dynamics, p. 39-46, Allyn and Bacon, 1969.

8. Gosman, A. D., Pun, W. M., Runchal, A. K. Spalding, D. B., and Wolfshtein, M., Heat and Mass Transfer in Recirculating Flows, Academic Press, 1969.

9. Spalding, D. B., Gosman, A. D., and Pun, W. M., The Prediction of Two-Dimensional Flows, Short Course, Pennsylvania State University, August 1972.

10. Holman, J. P., Experimental Methods for Engineers, 2nd edition, p. 37-44, McGraw-Hill, 1971.

11. National Advisory Committee for Aeronautics Report 1174, The Structure of Turbulence in Fully Developed Pipe Flow, by J. Laufer, p. 417-434, 1954.

12. Schlichting, H., Boundary Layer Theory, 6th edition, p. 531-537, McGraw-Hill, 1968.

INITIAL DISTRIBUTION LIST

		No. Copies
1.	Defense Documentation Center Cameron Station Alexandria, Virginia 22314	2
2.	Library, Code 0212 Naval Postgraduate School Monterey, California 93940	2
3.	Department Chairman, Code 57 Department of Aeronautics Naval Postgraduate School Monterey, California 93940	1
4.	Asst. Professor D. W. Netzer, Code 57Nt Department of Aeronautics Naval Postgraduate School Monterey, California 93940	2
5.	LCDR Joseph T. Phaneuf, USN FITRON One Twenty One NAS Miramar San Diego, California 92145	2

Thesis
P46176 Phaneuf
c.1
An experimental investigation of the internal ballistics of solid fuel ramjets.
155456